Raman scattering characterization of small semiconductor particles

岡田，正

(Degree)
博士（学術）

(Date of Degree)
1989-04-28

(Date of Publication)
2009-03-06

(Resource Type)
doctoral thesis

(Report Number)
乙1300

(URL)
https://hdl.handle.net/20.500.14094/D2001300

神戸大学博士論文

RAMAN SCATTERING CHARACTERIZATION OF SMALL SEMICONDUCTOR PARTICLES

（半導体微粒子のラマン散乱による評価）

By

Tadashi Okada

March, 1989

RAMAN SCATTERING CHARACTERIZATION OF SMALL SEMICONDUCTOR PARTICLES

Tadashi OKADA

Department of Electronics and Computer Engineering
Tsuyama National College of Technology

January, 1989

Abstract

This thesis makes a systematic study of the physical properties of small semiconductor particles of Si and Ge with a unified standpoint overlapping the small particle and amorphous semiconductor. There are main two purposes of this thesis work: One is to investigate finite-size effects on the vibrational modes in nonpolar semiconductors. The other is to contribute to the study of the structure of amorphous Si and Ge.

The investigation is carried out by using Raman scattering spectroscopy in combination with electron microscopy. The Raman spectra from the gas-evaporated Si particles with free boundary conditions are measured for the first time. The structural changes of the Si and Ge particles in thin films are detected and analyzed by the Raman scattering measurements successfully.

The author first demonstrates that the Si particles as small as 100 Å show an amorphous-like broad Raman spectrum even though their structure is crystalline. The particle size distribution, the electron diffraction patterns, the size dependence of the Raman spectrum are also discussed. The structure of the Si particles is checked by thermal annealing and laser irradiation experiments.

A structural change of evaporated Si films induced by thermal annealing is probed by Raman scattering. The two-step structural change with two activation energies is observed for the first time. The low energy obtained is the lowest value in those reported previously. The Raman scattering study is extended to glow-discharge-deposited Si films. Some comments are given on the theoretical studies dealing with the finite-size effects, and it is pointed out that the lack of proper theory at present.

The Raman depolarization ratio of small Si particles is measured for the first time. The result shows that bulk concepts are inoperative to the small Si particles, and the broad amorphous-like spectra do not mean the continuous random network structure or molecular-like cluster.

Germanium particles both with free boundary conditions and in thin film are studied by using the same analytical method as used for the Si particles. The two-step changes are observed showing the similarities between Si and Ge. Possible mechanisms of the two-step structural change are discussed based on the microcrystalline model instead of the continuous random network model.

Acknowledgment

The author is indebted to many individuals for making this thesis possible.

The author would like to acknowledge, first of all, Professor K. Yamamoto, who provided him the chance to enter the new world of this research field, of Kobe University for his constant guidance, encouragement and suggestions during every phase of this work.

The author would like to express his sincere thanks to Professor S. Hayashi of Kobe University for his valuable discussion, kind advice and critical reading of this thesis.

The author is also grateful to Professor T. Kanaji, Professor M. Motokawa, and Professor H. Matsumoto of Kobe University for their suggestions and guidance during the preparation of this thesis.

The author is indebted to many of his co-workers, most of whose names are found in his papers listed in the references, of Professor Yamamoto's laboratory for their help and useful discussions in this thesis work. In particular, the author takes pleasure in acknowledging the initial part played by Messrs. T. Iwaki and H. Kasahara.

The author wishes to thank Professor Y. Hamakawa of Osaka University for the preparation of glow-discharge deposited Si films and the measurement of X-ray diffraction.

The author also wishes to express special gratitude to the members of Tsuyama National College of Technology, especially Professors M. Nishiyama, S. Miki, S. Kishimoto, and J. Shimonishi, for their help and encouragement.

Finally, the author wishes to thank his wife Kyoko for her endless support and encouragement.

Contents

Chapter 1
Introductory Remarks

1.1 Small Particle Study

In our daily life, we live in a variety of powder and small particles. The rainbow, which occurs due to light scattering by atmospheric particles of rain drops, is one of the most impressive phenomena in nature. Our modern life is also surrounded by the industrial facilities utilizing powder or small particles. For example, black powders are indispensable to an electronic copier, and small magnetic particles are applied to media of magnetic recorders. In addition, small particles exist not only on the earth but also in interstellar space. An interstellar dust, the small particles sparsely populating the regions between stars, tells us valuable information on the birth and growth of stars. Thus a great interest in the small particles spreads over engineers and scientists from a surprising variety of disciplines; electrical engineering, solid-sate physics, chemistry, astronomy, meteorology, and biophysics.

In order to treat the small particles in a wide field, it is necessary to reveal the fundamental nature of the small particles. At present, however, we are far from the full understanding of the nature of the particles. The difficulty to understand the various properties of the small particles results from their smaller size than a usual size of bulk matter.

Since the properties of bulk matter are known to differ considerably from the atoms of which it is composed, it is expected that at some stage in the fragmentation of a bulk matter its properties begin to change drastically. Thus it is desired to construct new theoretical concepts and experimental techniques

for the research on the small particles. Now a new field in solid state physics grows aiming to study the physical properties of solids smaller than 1 μm in size, which are called by various terms such as small particles, ultrafine particles, microcrystals, nanocrystallites or microcrystallites.

In spite of the difficulty in treating theoretically and experimentally, the study of scattering and absorption of light by small particles is one of the most successful field. Because the scattering and absorption of light by small metallic particles result in the brilliant colors of stained glasses, the optical properties of small particles have been the subject of intense investigations from the late nineteenth century.[1] A wide variety of optical spectra of small particles can be explained in terms of special electromagnetic oscillation in the particles, called electromagnetic surface modes or surface polaritons.[2] The concept of the surface polaritons is extended to other particles such as semiconductor ones, and has been successful in explaining experimental results. For example, Hayashi[3] has summarized the theories of the surface modes in the small particles and has showed how the surface modes can be identified experimentally for infrared spectra of MgO particles and Raman spectra of GaP particles.

It is noted that the success of surface modes in semiconductor particles is limited to small ionic crystals. The notion of electromagnetic surface modes is valid only for polar phonon modes. However in the semiconductor particles nonpolar materials such as Si and Ge are very important because finite-size effects on the nonpolar particles must be clarified to realize microdevices. Therefor the vibrational and optical properties has been the subject of rather intense investigations in recent

years.

1.2 Amorphous Semiconductor Study

Amorphous materials, mainly oxide glasses, are abundant as much as small particles in nature. Before the last two decades, the interest in amorphous materials has lain in the thermodynamical and structural aspects as a solid in the vitreous states or the quantum statistical studies as a random network system. Now much attention is devoted to amorphous materials, mainly amorphous semiconductors, from view point of solid state physics aimed for the practical application to electronic devices.

This drastic change results from the discovery of the valency controllability in glow-discharge-produced amorphous silicon by Spear and LeComber in 1975.[4] Since then, a considerable amount of intensive investigations has been carried out on the preparation technology, the electronic properties of amorphous silicon and related materials. Nowadays intensive efforts have produced various practical devices utilizing amorphous silicon such as low-cost solar cells, thin films transistors, and integrated photosensors.

For the amorphous silicon as well as the other amorphous materials, the chemical bonding structure is one of the most important property to clarify the basic nature. The bonding configurations have been investigated by the vibrational properties through Raman and infrared spectroscopy. In fact, the vibrational modes measured in Raman and infrared spectra have revealed the local bonding environment and the role of incorporated atoms.[5-7] The observation obtained by the vibrational study has contributed effectively toward improving the device

characteristic.

Although amorphous semiconductors have been used successfully in the application field, there is a controversy in a fundamental aspect of the structural models. A conflict between the two models, i.e. a microcrystalline model and a continuous random network model, has been made. It seems that the continuous random network model has generally been favored in Western papers. However a few analyses in formative data obtained by, mainly, high-resolution transmission electron microscopy have supported the microcrystalline model.[8,9] Therefor further studies are desired to confirm the structural models by using a variety of experimental methods and theoretical approach.

1.3 Scope of the Present Work

As mentioned in the preceding sections, investigations of both the finite-size effects on physical properties of small particles and the structure of amorphous solids are important for not only a basic research but also an applied field. However, up to this time, no one considered in connection with the small semiconductor-particle study and the amorphous semiconductor study. The author pointed out for the first time that the studies overlapping the above two fields are possible by considering small particles or microcrystals for nonpolar semiconductors, Si and Ge elements.

The purpose of this thesis work is to carry out a systematic investigation on small semiconductor particles and amorphous semiconductors with a unified standpoint. A considerable effort is paid to inquire into the appearance of finite-size effects of Si and Ge substances on the vibrational properties. The vibrational properties are examined experimentally by, mainly, using

Raman scattering measurement. The vibrational modes are also used to analyze the structural changes of Si and Ge films.

In chapter 2, the author gives the preparation method and the particle-size analysis of gas-evaporated small silicon particles. The particle-size dependence of Raman spectra of the Si particles is discussed in connection with their electron diffraction patterns.[10,11] Then changes in the Raman spectrum induced by thermal annealing or laser irradiation are examined to clarify the structure of the Si particles.[12-15]

Chapter 3 deals with the small Si particles in thin films. Changes in the Raman spectra of evaporated[14,16] and glow-discharge deposited[17] thin Si films are discussed in terms of the peak frequency and linewidth of a TO-like mode and a volume fraction of crystallinity. The effects of thermal annealing for the evaporated films and of the deposition conditions for the glow-discharge deposited film on the Raman spectra give us the structural information of the Si films.

In chapter 4, a comparative study of Si particles and films is given by using the measurement of the Raman depolarization ratio.[18] The result presented in this chapter shows that the polarization properties of the Si films are not interpreted by the continues random network model but favor the microcrystalline model instead.

In chapter 5, the investigation dealing with the small Si particles is extended to small germanium particles.[19,20] The same analytical procedures as used for the Si particles are applied to the structural interpretation of Ge particles and films. The results obtained in this chapter agree with those described in the preceding chapters.

In the final chapter, some conclusions obtained through this

thesis work are summarized.

References

1) C. F. Bohren and D. R. Huffman: *Absorption and Scattering of Light by Small Particles* (Wiley-Interscience, New York, 1983).

2) A. D. Boardman (ed.): *Electromagnetic Surface Modes* (Wiley-Interscience, New York, 1982).

3) S. Hayashi: Jpn. J. Appl. Phys. 23 (1984) 665.

4) W. E. Spear and P. G. LeComber: Solid State Commun. 17 (1975) 1193.

5) T. Okada and K. Yamamoto: Bull. Tsuyama Natl. Coll. Tech. 22 (1984) 23.

6) T. Okada and K. Yamamoto: Bull. Tsuyama Natl. Coll. Tech. 23 (1985) 25.

7) T. Okada and K. Yamamoto: Bull. Tsuyama Natl. Coll. Tech. 24 (1986) 19.

8) Y. Saito: J. Phys. Soc. Jpn. 53 (1984) 4230.

9) J. C. Phillips, J. C. Bean, B. A. Wilson and A. Ourmazd: Nature 325 (1987) 121.

10) T. Okada, T. Iwaki, K. Yamamoto, H. Kasahara and K. Abe: Solid State Commun. 49 (1984) 809.

11) T. Okada, T. Iwaki, H. Kasahara and K. Yamamoto: J. Phys. Soc. Jpn. 54 (1985) 1173.

12) K. Yamamoto, T. Okada, T. Iwaki and H. Kasahara: *Proc. 9th Int. Conf. Raman Spectrosc., Tokyo, 1984,* (Organizing Committee for The IX th International Conference on Raman Spectroscopy, 1984) p.234.

13) T. Iwaki, T. Okada, H. Kasahara and K. Yamamoto: *Proc. 4th Symp. Ultrasonic Electronics, Tokyo, 1983,* Jpn. J. Appl. Phys. 23 (1984) Suppl. 23-1, p.72.

14) T. Okada, T. Iwaki, H. Kasahara and K. Yamamoto: Solid State

Commun. 52 (1984) 363.

15) T. Okada and K. Yamamoto: Jpn. J. Appl. Phys. 26 (1987) 2134.

16) T. Okada, T. Iwaki, H. Kasahara and K. Yamamoto: Jpn. J. Appl. Phys. 24 (1985) 161.

17) T. Okada and K. Yamamoto: IECEJ Tech. Rep. SSD84-158 (1985-3) 75 [in Japanese].

18) T. Okada, H. Sasaki, S. Hayashi, S. S. Kim and K. Yamamoto: Solid State Commun. 61 (1987) 671.

19) T. Okada, H. Wakayama, H. Kasahara and K. Yamamoto: J. Phys. Soc. Jpn. 55 (1986) 1415.

20) S. Hayashi, H. Wakayama, T. Okada, S. S. Kim and K. Yamamoto: J. Phys. Soc. Jpn. 56 (1987) 243.

Chapter 2
Gas-Evaporated Small Silicon Particles

2.1 Introduction

Finite-size effects on the polar vibrational excitations of small ionic crystals have been discussed in a number of experimental and theoretical studies. The status of this research area was surveyed in 1970 by Ruppin and Englman,[1] and recently by Hayashi.[2] An essential feature of the finite-size effects is the appearance of surface phonon modes or surface polaritons, which have been predicted by an electromagnetic theory.[3,4] Experimental observation of the surface phonon modes has been made for small crystals of various materials, *e.g.* ZnO,[5,6] MgO,[7-9] and GaP,[10] by infrared absorption[5-7,9] or Raman scattering[8,10] measurement; the results have been successfully interpreted in terms of the Mie theory[1,11] and an effective medium theory.[12,13] In addition, the coupling between surface phonons and surface plasmons has been reported for the small crystals of CdO,[14] GaN,[15] and GaAs.[16] However as mentioned in § 1.1, the investigation concerned with the finite-size effects were restricted to polar modes in ionic crystals; only a few studies of the finite-size effects have been made for nonpolar materials such as graphite[17] and boron nitride.[18]

On the other hand, microcrystalline silicon as well as germanium have received current interest in a field of amorphous semiconductors. The microcrystalline Si and Ge are uncritically supposed to be the materials consisting of microcrystals embedded in amorphous matrix, but these structural models are in controversy. In the studies of these materials, Raman scattering has been used to characterize the structural order of amorphous

film[19-21] and the changes in the Raman spectra due to the variation of crystallite size have been reported.[22-24] However all experiments on microcrystals have been carried out in the form of film; the Raman spectra of the small particles with free boundary conditions have been measured only for germanium.[25]

Stimulated by the situation mentioned above, we carried out a systematic experiment on the Raman scattering from the small silicon particles prepared by gas-evaporation technique.[26,27] As far as the author know, this work is the first experiments on the small Si particles with free boundaries. Accordingly, we report the effect of particle size on the Raman spectra of the Si particles in connection with an electron diffraction study. We find that the Si particles possess the same crystalline structure as the bulk Si in spite of their amorphous-like Raman spectra. Moreover, we reveal the spectral structure by resolving the Raman spectra, and propose a new surface mode whose integrated intensity decreases with an increase of the particle size. The behavior of Raman spectrum induced by thermal annealing or laser irradiation is also measured to clarify the structure of the Si particles.[28-31]. Finally, some comments on the theoretical studies related to the present experiment are given, suggesting a lack of proper theory to account for the results fully.

2.2 Experimental

The small silicon particles were prepared by the customary gas-evaporation technique,[32,33] in which bulk materials are evaporated in an inert gas at a low pressure. In the present experiment, crystalline silicon chips were evaporated from a boron nitride boat in an argon gas. A schematic diagram of the

preparation system is shown in Fig. 2.1. In order to obtain much smaller particles than those obtained previously,[33] a series of experiments was carried out at pressures below 1 Torr, which were one or two orders of magnitude lower than the customary condition.[33]

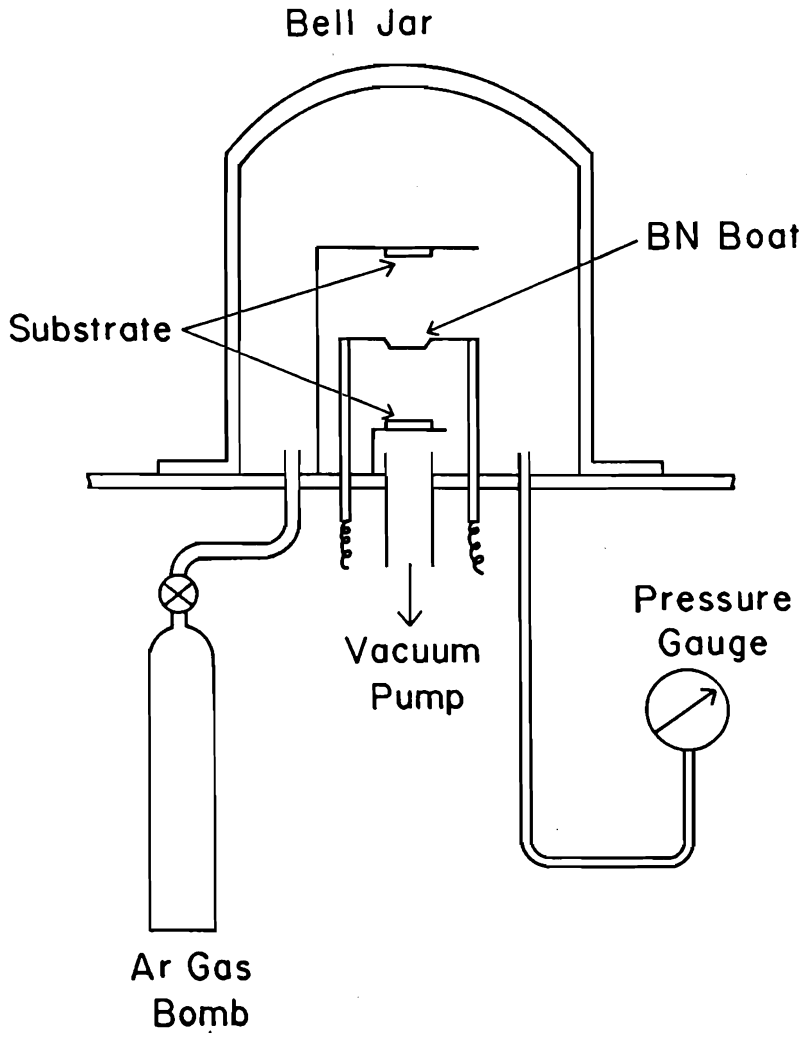

Fig. 2.1 Schematic diagram of the preparation system of small silicon particles.

The particle size was controlled by the argon gas pressure, with constant conditions of the evaporation temperature and the distance between the boron nitride boat and the substrate. The gas pressure was varied from 0.1 to 1 Torr for the samples of the size dependence experiment, and was kept at 0.17 Torr for the samples of the thermal annealing and the laser irradiation experiments.

The silicon powder was collected onto the substrates of various materials: glass covered with evaporated thin aluminum film, quartz, sapphire, single crystal silicon, and tungsten. The differences in the Raman spectra measured were hardly observed among the substrate materials, except for single crystal silicon used in the thermal annealing (see the later discussion in § 2.5). Thus the results reported in this chapter were mostly obtained from the samples collected onto the glass covered with the aluminum film for as-deposited measurement because of a complete absence of the scattering maxima from the substrate and a reduction of background noise. On the other hand, the samples collected onto the quartz, which was stable during the heat treatment, were used for the thermal annealing and the laser irradiation experiments.

The thermal annealing was carried out in a quartz tube evacuated down to pressure of the order of 10^{-6} Torr. The tube containing the samples was inserted in an electric oven. The annealing temperature was kept at a constant value within 2 % in a range of 100 to 800 °C. The annealing time was fixed at 30 minutes for all results reported here. The samples annealed at the desired temperature were quenched to room temperature in the vacuum.

In the Raman scattering measurements, we used a SPEX RAMALOG

5M double monochromator with standard cooled photomultiplier and photon counting system. The measurements were made at room temperature in a convenient 90° scattering geometry with 4880 Å line of an argon ion laser as an exciting source. The laser power used for the size dependence and the thermal annealing experiments was less than 50 mW to prevent a local heating of the samples, because we observed that no changes is detectable for samples irradiated at a laser power below 50 mW. In laser irradiation experiment, leaving a margin we used a power of 30 mW as the condition under which the temperature of a sample is considered to be at room temperature, and carried out an experiment for laser heating at powers above 80 mW.

Subsequently, the powder samples collected on a microgrid coated with a carbon thin film were studied by a JEM-200CX (JEOL) electron microscope operated at 200 kV. According to the usual manner,[10,34] the micrographs obtained were used to determine the average particle size d of small Si particles. The electron diffraction patterns were also measured.

The Raman spectra for the particle-size dependence were analyzed by a Du Pont 310 Curve Resolver. The spectra could be resolved into several components in a range of 250 to 600 cm^{-1}, assuming Gaussian lineshapes. This analysis was suitable to reveal spectral changes, and has been successfully applied to probe the crystallinity of evaporated Si film as shown in Chapter 3.

2.3 Size Analysis and Electron Diffraction

The average particle size d determined from the micrograph varies from 70 to 220 Å with increasing the argon gas pressure from 0.1 to 1 Torr. It is noted that the values observed are

similar to the size of microcrystals observed in microcrystalline silicon films.[22,23]

To deduce the growth kinetics of the silicon particles, we examine the size distribution. A representative size histogram for the sample prepared at the pressure of 0.5 Torr is shown in Fig. 2.2. It has been known[34,35] that the size distribution of inert-gas-evaporated particles is well described by a log-normal distribution function:

$$f(d_x) = \frac{1}{(2\pi)^{1/2} \ln\sigma} \exp\left[- \frac{(\ln d_x - \ln d)^2}{2 \ln^2\sigma} \right], \qquad (2.1)$$

where d_x and σ are the individual particle size and the geometric standard deviation. This log-normal curve is also plotted in Fig. 2.2; the curve calculated from the experimental values listed in the caption reproduces fairly well the histogram. Moreover, σ agrees with an empirical rule for the width of the distribution. That is, regardless of the materials, σ has to fall within a band given by $\sigma = 1.48 \pm 0.2$ for crystalline inert-gas-evaporated particles; although silicon is excluded from the consideration,[34,35] the same is true for the Si particles investigated here ($\sigma = 1.39$).

The above result implies[34] that the Si particles are formed by the following process: The atoms effused from the heated vapor source lose their energy rapidly by collision with the gas atoms, the stable clusters of the atoms are produced by homogeneous nucleation, and those embryonic particles then grow by liquid-like coalescence to form large grains. This is the first observation of the log-normal distribution for the size of Si particles.

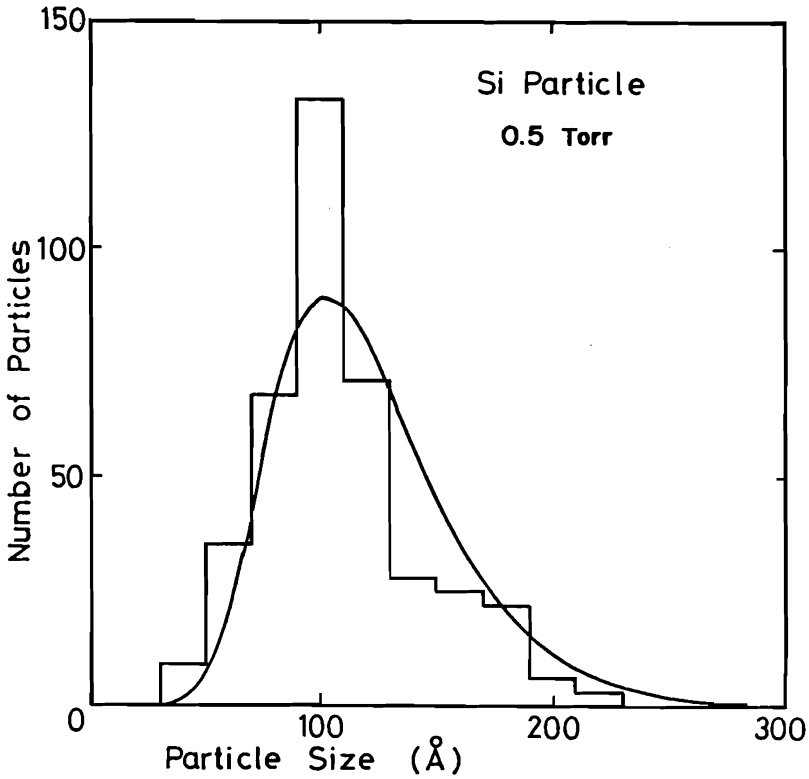

Fig. 2.2 Size distribution for the silicon particles prepared at the pressure of 0.5 Torr. The staples denote the number of particles counted per size interval 20 Å. The bell-shaped curve represents a fit to a log-normal distribution function characterized by the following values: d = 103 Å and σ = 1.39, where d and σ are the statistical median and the geometric standard deviation. The area under the curve is put equal to the area under the histogram, 400 particles × 20 Å.

Next, we show in Fig. 2.3 two electron diffraction patterns obtained from the samples having d = 70 (the left) and 220 Å (the right) corresponding to, respectively, the smallest and the largest ds produced in the present experiment. Debye-Scherrer rings are clearly observable even for the samples with d = 70 Å, and the bright spots are often found for the samples prepared at higher pressure. An analysis of these diffraction patterns shows that the Si particles have the ordinary diamond structure; the lattice parameters calculated from (111), (220) and (311) planes are 5.41, 5.40 and 5.43 Å respectively, and agree with the standard value of silicon (5.43 Å) within an experimental accuracy.

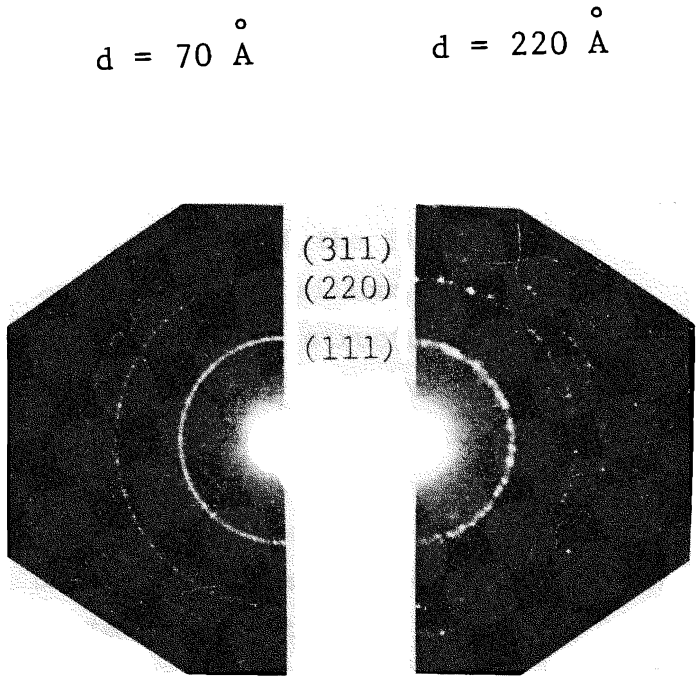

Fig. 2.3 Electron diffraction patterns of the silicon particles with d = 70 (the left) and 220 Å (the right).

From the results presented above, we can conclude that the Si particles possess the same inner structure as the bulk crystalline Si. In this context, the present silicon particles are termed the silicon microcrystals reasonably.

2.4 Size Dependence of Raman Spectra

In the preceding section, it was shown that the silicon particles possess the crystalline structure. In contrast to this result, the Raman spectra of the Si particles change from an amorphous-like broad spectrum (d = 70 Å) to a mixed spectrum with crystalline and amorphous-like phases (d = 220 Å). This size dependence is shown in Fig. 2.4. It is somewhat similar to the case of microcrystalline Si films[22,23] that the crystalline mode at the frequency of slightly below 520 cm^{-1} grows with increasing d. However, the spectra are not identical to those of the films; for example, the shift of an apparent peak position in Fig. 2.4 is large compared with that of the films containing the same size of microcrystals.[22,23] Furthermore, the "amorphous-like" spectrum of the Si particles differs substantially from that of amorphous silicon films.[30]

To clarify the spectral structure, we resolved the Raman spectra into several components; two typical resolved spectra are shown in Fig. 2.5. The resolved components are classified into four modes based on the center frequency in the range of 250 to 600 cm^{-1}. The relative integrated intensity I (the percentage area of the individual component to the total area) of each mode is plotted as a function of d in Fig. 2.6. In the following discussion, each relative integrated intensity I is designated by the subscript of the center frequency.

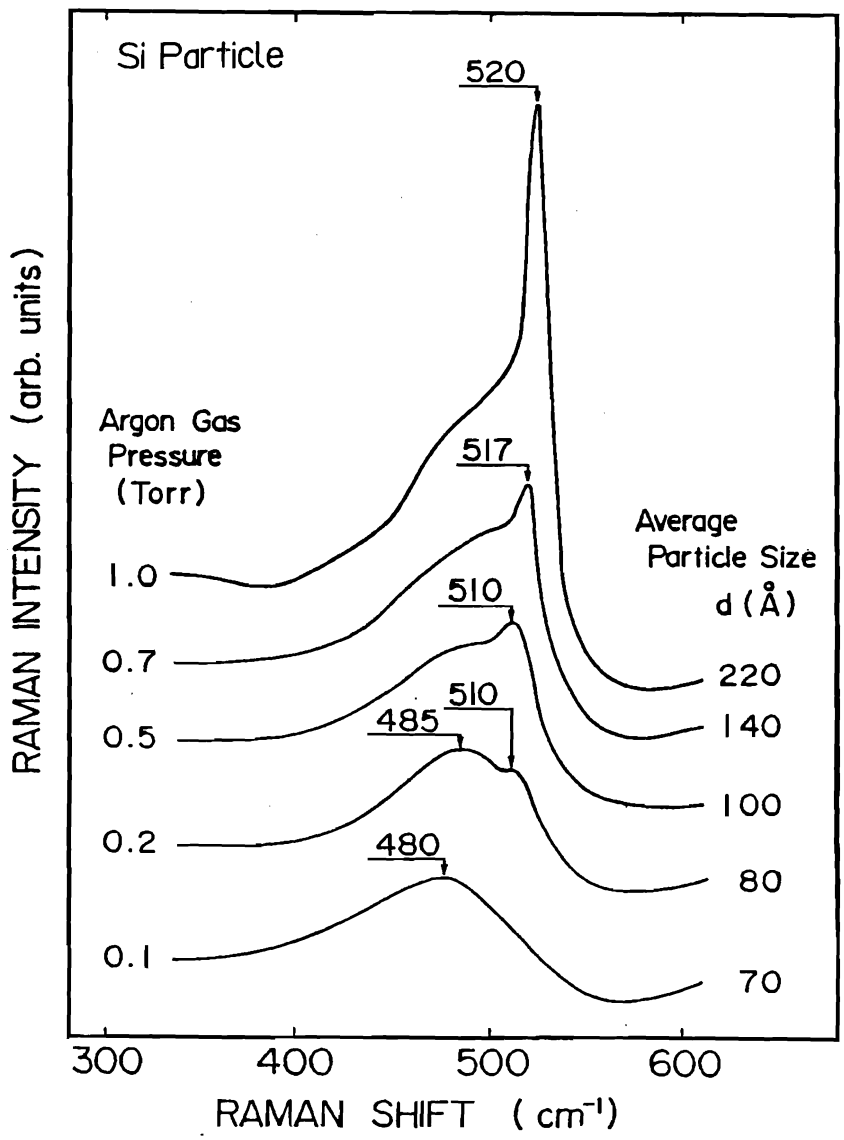

Fig. 2.4 Size dependence of the Raman spectra of the silicon particles. The values indicated by directed lines are peak frequencies in cm^{-1}.

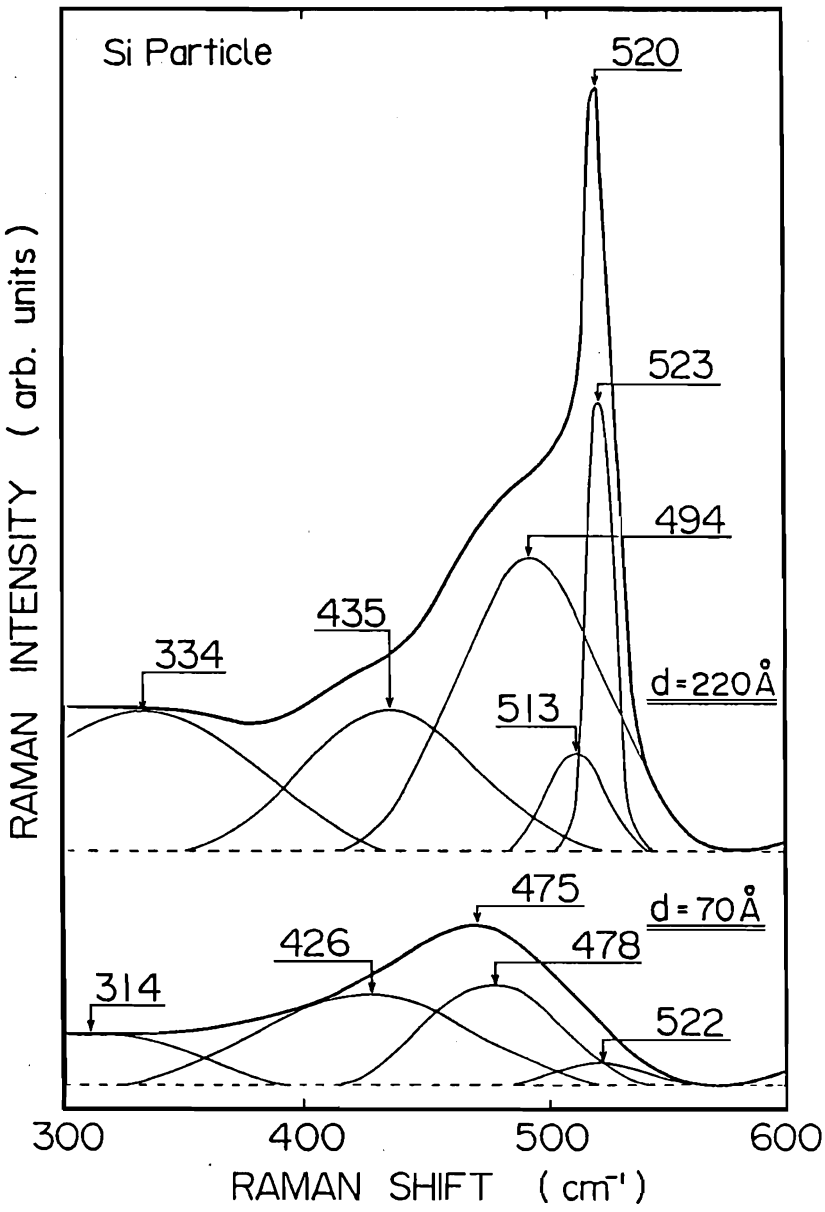

Fig. 2.5 Two typical resolved spectra for the samples with d = 70 and 220 Å.

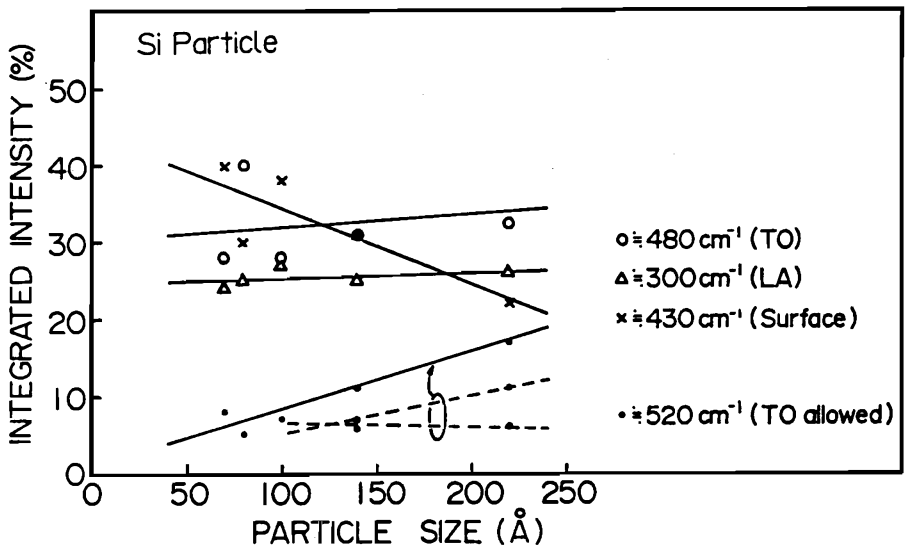

Fig. 2.6 Dependence of the relative integrated intensities Is of the resolved modes on the average particle size d. The solid lines are least-squares fits to the experimental points. In our resolving procedure, the errors of I and the center frequency are estimated to be about 5% and 10 cm^{-1}, respectively.

We shall begin with the identification of the four modes. As is clearly seen in Fig. 2.6, I_{300} and I_{480} are nearly constant independently of d. Because of these tendencies and their frequencies, we assign these modes to LA- (I_{300}) and TO- (I_{480})

like-phonon modes observable in amorphous silicon.[20] On the other hand, since I_{520} increases as d increases, this mode is assigned to the allowed-TO-phonon mode of crystalline silicon,[36] which means the mode arising from the allowed Γ_{25}' symmetry $q \sim 0$ optical phonon. In relation to this mode, it should be noted that the allowed-TO modes of the samples having $d > 100$ Å are composed of two parts; these are shown by broken lines in Fig. 2.6. One mode with higher frequency is narrower than the other lower mode and appears in the sample of large d. It is worth noting that the same split has already been observed in the Raman spectra of microcrystalline silicon films.[37-39] For this split of the crystalline mode, we tentatively give our interpretation as follows: The narrower mode due, certainly, to the wave-vector selection rule appears only when the particles are sufficiently large to regard them as single crystals for Raman event, while the broader mode occurs in relatively small crystalline particles and the shift to low frequency of this mode arises from finite-size effects discussed below.

In contrast to the modes stated above, the remaining mode with the frequency of 430 cm^{-1} has a different character, i.e. a decrease of I_{430} with an increase of d. Although LO-like mode of amorphous silicon was observed at about 380 cm^{-1},[20] we can not accept the assignment of I_{430} to the LO-like mode because I_{430} is very different from I_{300} and I_{480} in size dependence and the LO-like signal of amorphous silicon was frequently much weaker than those of the other modes.[40] Consequently, we assign this mode to a new surface mode; this term comes from its character that the surface contribution due to decreasing d appears as the increasing of I_{430}.

The result stated above indicates that the Si particles as

small as 100 Å show a amorphous-like Raman spectrum even though their structure is crystalline. To interpret this observation, we refer to some theoretical studies to account for the Raman spectra of amorphous and/or microcrystalline silicon.[23,24,41-43] These calculations are based on a relaxation of the wave-vector selection-rule[23,24,43] or normal mode calculation.[41,42] The main motivation of the recent studies[23,24,43] is to explain the red shift as well as the broadening of the Raman allowed mode; this aim is achieved in semiquantitative fashion. In particular, the result of the calculation based on the relaxation of the wave-vector selection-rule[24,43] is able to explain the observation of the shift and the broadening of the Raman allowed mode obtained from highly crystallized silicon films (see Chapter 3).

As to the Raman spectra of the small Si particles with the free boundary condition, non of the studies give us an overall agreement with the experimental results, especially the amorphous-like spectra of the particles with the crystalline structure and the spectral structure involving the surface mode. The disagreement between the theoretical studies and the experimental one is due, presumably, to the lack of the full consideration to important effects such as a proper surface contribution and a size distribution encountered in real samples. The attempt to interpret the amorphous-like Raman spectra has suggested by considering the contribution from the free surface layers of the small particles.[44,45] In the present time, however, the full understanding is not yet achieved. So further experimental and theoretical studies will be required to account fully for the observed results. For this purpose the present work may give some information to one who will investigate the

subject.

2.5 Annealing Behavior of Raman Spectra

In order to check the structure of the silicon particle, it is useful to examine whether the Raman spectra of the silicon particles are affected by the thermal annealing[28-30] and laser irradiation.[28,31]

The result of the isochronal annealing experiment on the Si particles is shown in Fig. 2.7. The change in the Raman spectra by the annealing is slight over the whole temperature range. We believe that this is caused by the stability of the particle with the crystalline structure. Next, we resolved the Raman spectra in Fig. 2.7 by using the same procedure as applied in § 2.4. The small change induced by the annealing can be resolved in the region between the surface and TO-like modes as a broad component (~ 450 cm^{-1}), together with the other modes discussed in § 2.4. The dependence of the relative integrated intensities of the TO-like, the surface and the additional modes on the annealing temperature is shown in Fig. 2.8. The origin of this additional mode is attributed to the formation of Si-O bond on the surface by its dependence of the relative integrated intensity on the annealing temperature.[30] That is, this mode results from the vibration of the oxygen atom along a line bisecting the Si-O-Si angle, which has been the subject of theoretical and experimental investigations on vitreous silica.[46-49] Thus we conclude that a slow rise of temperature forms the oxidation layer on the surface of the crystalline particle and each particle remains separately.

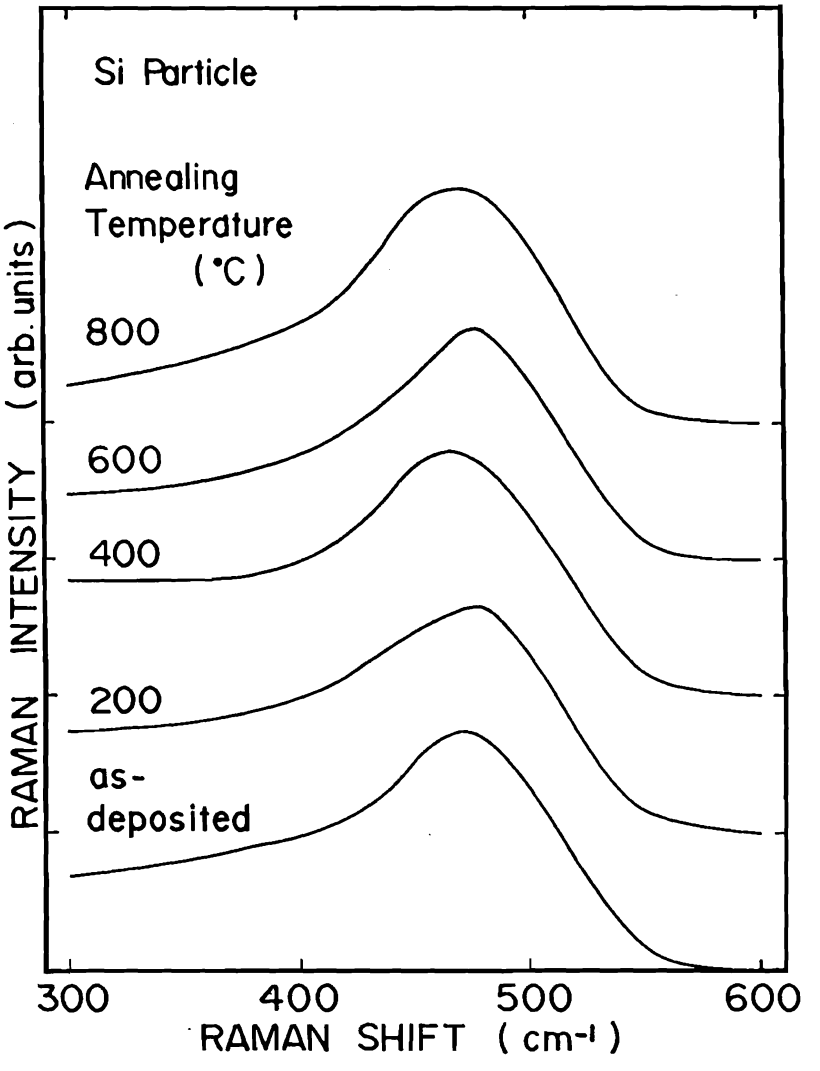

Fig. 2.7 Dependence of the Raman spectra of the silicon particles annealed thermally on the isochronal annealing temperature.

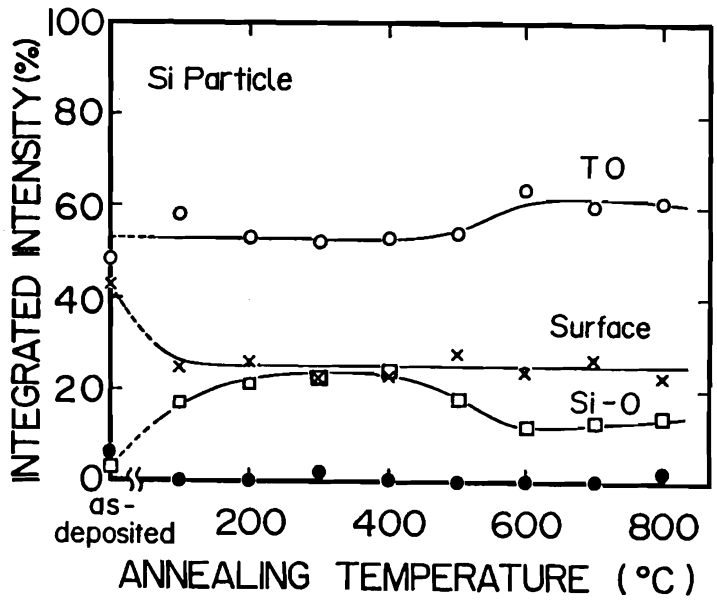

Fig. 2.8 Dependence of the relative integrated intensities of the TO-like, the surface and the additional modes on the annealing temperature. As to "Si-O" mode, see the text.

In contrast to the thermal annealing, the laser irradiation induces the sharp crystalline peak on the Raman spectrum of the Si particles. The observed changes are considered to indicate an increase in the grain size of particles as a laser annealing effect, because a high energy of the laser yields a rapid rise of temperature. That is, the growth of particles is produced by laser heating in a manner like the surface melting coalescence discussed in Chapter 5.

To estimate the elevated temperature during laser irradiation, we use the relationship between the peak frequency shift

and the linewidth of the Raman spectrum. For the same sample, we measured the Raman spectra at high-power irradiation (above 80 mW) and at a low-power level (30 mW) after cooling. An example of two Raman spectra for the high- and low-power levels is shown in Fig. 2.9. At the high-power level, the Raman spectrum shifted to the lower-frequency side and became broad; this frequency shift and the broadening apparently indicate a rise in temperature during laser irradiation. To quantitatively estimate the temperature, we assume that the temperature dependence of the frequency shift and the linewidth (a full width at half maximum) of the Raman spectrum from the Si particles is the same as that for bulk Si. This assumption is reasonable because of the discussion stated in this chapter that the Si particles are crystalline.

We then compared our observed values with the theoretical result reported by Balkanski *et al.*[50] Their calculation included contributions from four-phonon anharmonic processes and has provided a good fit to the experimental values for the frequency shift and the linewidth up to 1400 K. It is, therefore, appropriate to compare our results.

Figure 2.10 shows a comparison between the theoretical line for bulk Si and the measured points for the Si particles as a relationship between the peak frequency shift and the linewidth. The damping constant (the linewidth according to our term) Γ and the frequency shift Δ are specified as a function of temperature T by the expressions[50]

$$\Gamma(T) = A\left[1 + \frac{2}{e^{x} - 1}\right] + B\left[1 + \frac{3}{e^{y} - 1} + \frac{3}{(e^{y} - 1)^{2}}\right], \tag{2.2}$$

and

$$\Delta(T) = C\left[1 + \frac{2}{e^{x} - 1}\right] + D\left[1 + \frac{3}{e^{y} - 1} + \frac{3}{(e^{y} - 1)^{2}}\right], \tag{2.3}$$

where $x = h\omega_0/4\pi k_B T$, $y = h\omega_0/6\pi k_B T$, h is the Planck's constant, k_B Boltzmann constant, ω_0 the Raman frequency (528 cm^{-1} for the present case), and A, B, C, and D are constants founded by Balkanski *et al.*[50] to be 1.295, 0.105, - 2.96, and - 0.174 cm^{-1} respectively. The theoretical line potted in Fig. 2.10 was derived from eqs. (2.2) and (2.3) by eliminating the parameter T. An additional assumption was made in order to plot the experimental points; that all finite-size effects are included in the low-power spectrum. Thus the differences in the peak frequency shift and the linewidth arise only from the temperature rise from room temperature.

It is evident that the agreement between the experimental points and the theoretical line is fairly good in spite of our simple treatment. In addition we can estimate the elevated temperature during laser irradiation from Fig. 2.10; for example, at a power of 300 mW the temperature is estimated to be 1106 K. We thus conclude that the change observed in the Raman spectrum of the small Si particles during laser irradiation is caused by a temperature rise in the same manner as that which takes place in bulk Si. This is consistent, together with the conclusion from the thermal annealing results, with our opinion that the small Si particles are crystalline.

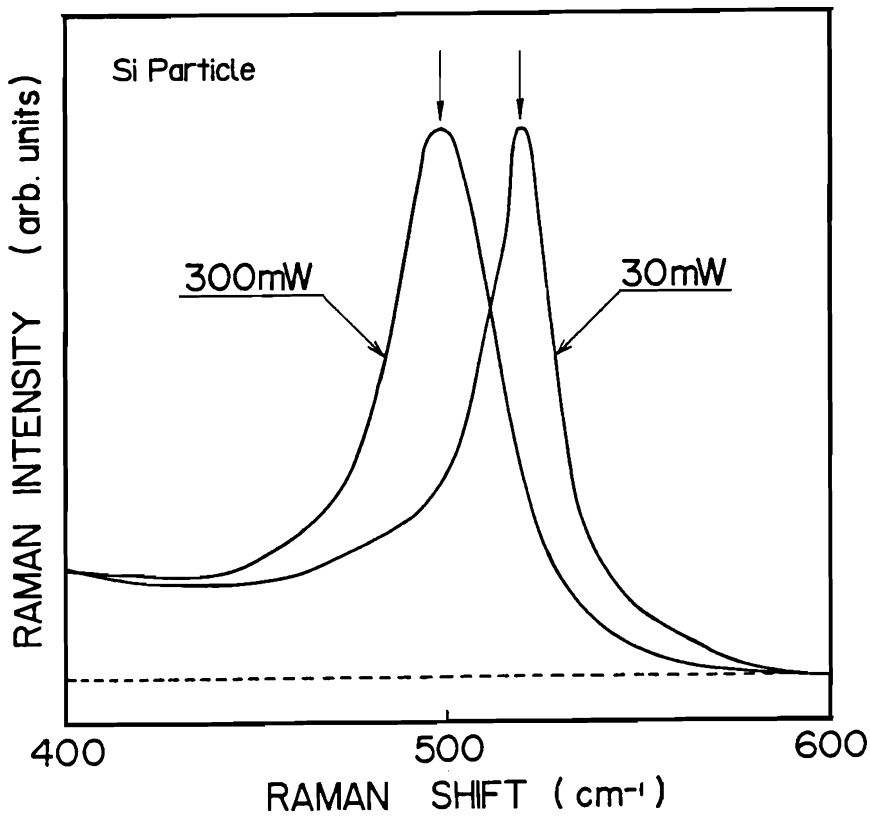

Fig. 2.9 Differences in the Raman spectra of the same sample at two laser-power levels (30 and 300 mW). The two spectra are normalized to the maximum intensity. Vertical arrows indicate the peak frequencies.

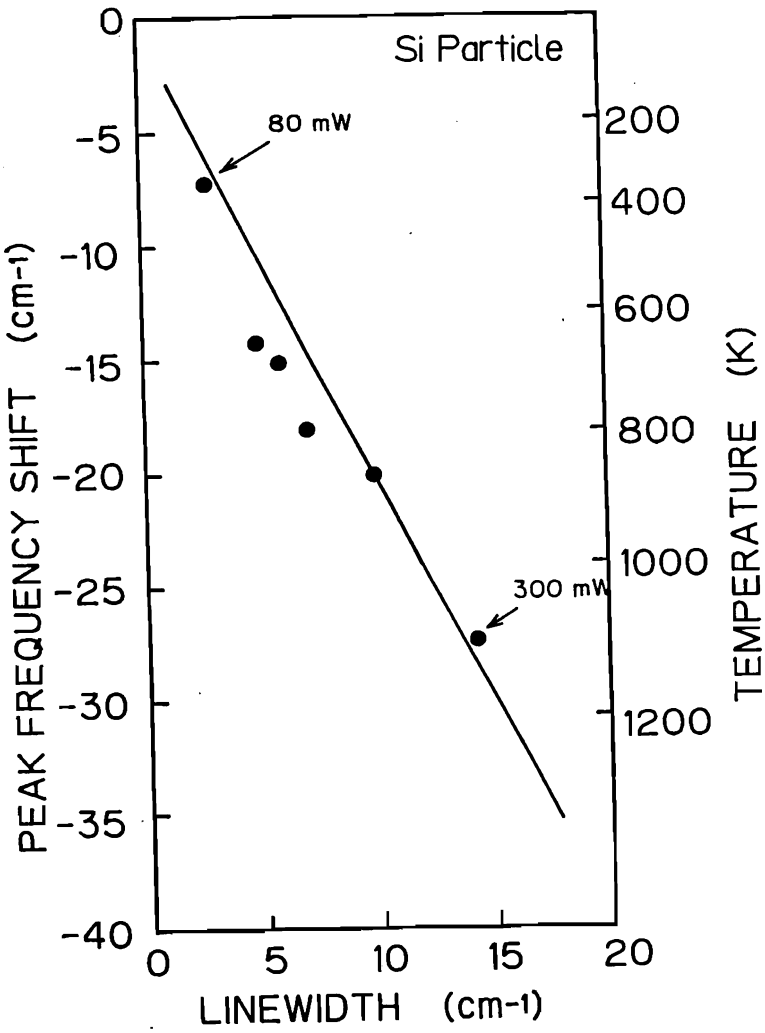

Fig. 2.10 Relationship between the peak frequency shift and the linewidth accompanying a temperature variation. The solid line was derived from the theoretical calculation reported by Balkanski *et al.*[50] The circles designate the experimental points.

2.6 Summary

In order to examine the finite-size effects of small particles with free boundary condition, we measured for the first time the Raman spectra from the small Si particles prepared by gas evaporation technique. The electron microscopic study showed that the size distribution of the Si particles is well described by a log-normal distribution function, and that the Si particles possess the crystalline structure.

The particle-size dependence of the Raman spectra was clearly observed and analyzed by resolving the spectra into a new surface mode and three known modes. It was noted that the Si particles as small as 100 Å show an amorphous-like broad Raman spectrum even though their structure is crystalline. We commented some theoretical studies to interpret this observation; however we mentioned that the full understanding to account for the observed results is not yet achieved.

The effects of the thermal annealing and the laser irradiation on the Raman spectra of the Si particles were also discussed to check the structure of the Si particles. Both results were interpreted by considering the structure of the Si particles as the crystalline one.

References

1) R. Ruppin and R. Englman: Rep. Progr. Phys. 33 (1970) 149.
2) S. Hayashi: Jpn. J. Appl. Phys. 23 (1984) 665.
3) R. Fuchs and K. L. Kliewer: J. Opt. Soc. Am. 58 (1968) 319.
4) R. Englman and R. Ruppin: J. Phys. C: Solid State Phys. 1 (1968) 614.
5) K. Yamamoto, D. C. Tran, H. Shimizu and K. Abe: J. Phys. Soc. Jpn. 42 (1977) 587.
6) K. Yamamoto, K. Ueda, M. Yamada and K. Abe: J. Phys. Soc. Jpn. 46 (1979) 1792.
7) L. Genzel and T. P. Martin: Phys. Status Solidi b 51 (1972) 91.
8) H. K. Böckelmann and R. G. Schlecht: Phys. Rev. B 10 (1974) 5225.
9) S. Hayashi, N. Nakamori, J. Hirono and H. Kanamori: J. Phys. Soc. Jpn. 43 (1977) 2006.
10) S. Hayashi and H. Kanamori: Phys. Rev. B 26 (1982) 7079.
11) G. Mie: Ann. Phys. (Germany) 25 (1908) 377.
12) L. Genzel and T. P. Martin: Surf. Sci. 34 (1973) 33.
13) S. Hayashi, N. Nakamori and H. Kanamori: J. Phys. Soc. Jpn. 46 (1979) 176.
14) K. H. Rieder, M. Ishigame and L. Genzel: Phys. Rev. B 6 (1972) 3804.
15) R. Ruppin and J. Nahum: J. Phys. & Chem. Solids 35 (1974) 1311.
16) K. Yamamoto, K. Kimura, M. Ueda, H. Kasahara and T. Okada: J. Phys. C: Solid State Phys. 18 (1985) 2361.
17) R. J. Nemanich and S. A. Solin: Phys. Rev. B 20 (1979) 392.
18) R. J. Nemanich, S. A. Solin and R. M. Martin: Phys. Rev. B 23 (1981) 6348.

19) M. H. Brodsky: *Light Scattering in Solids,* ed. M. Cardona (Springer-Verlag, Berlin and New York, 1975), p.205.

20) D. Bermejo and M. Cardona: J. Non-Cryst. Solids 32 (1979) 405.

21) Y. Hishikawa, K. Watanabe, S. Tsuda, M. Ohnishi and Y. Kuwano: Jpn. J. Appl. Phys. 24 (1985) 385.

22) Z. Iqbal, S. Veprek, A. P. Webb and P. Capezzuto: Solid State Commun. 37 (1981) 993.

23) Z. Iqbal and S. Veprek: J. Phys. C: Solid State Phys. 15 (1982) 377.

24) I. H. Campbell and P. M. Fauchet: Solid State Commun. 58 (1986) 739.

25) S. Hayashi, M. Ito and H. Kanamori: Solid State Commun. 44 (1982) 75.

26) T. Okada, T. Iwaki, K. Yamamoto, H. Kasahara and K. Abe: Solid State Commun. 49 (1984) 809.

27) T. Okada, T. Iwaki, H. Kasahara and K. Yamamoto: J. Phys. Soc. Jpn. 54 (1985) 1173.

28) K. Yamamoto, T. Okada, T. Iwaki and H. Kasahara: *Proc. 9th Int. Conf. Raman Spectrosc., Tokyo, 1984,* (Organizing Committee for The IX th International Conference on Raman Spectroscopy, 1984) p.234.

29) T. Iwaki, T. Okada, H. Kasahara and K. Yamamoto: *Proc. 4th Symp. Ultrasonic Electronics, Tokyo, 1983,* Jpn. J. Appl. Phys. 23 (1984) Suppl. 23-1, p.72.

30) T. Okada, T. Iwaki, H. Kasahara and K. Yamamoto: Solid State Commun. 52 (1984) 363.

31) T. Okada and K. Yamamoto: Jpn. J. Appl. Phys. 26 (1987) 2134.

32) K. Kimoto, Y. Kamiya, M. Nonoyama and R. Uyeda: Jpn. J.

Appl. Phys. 2 (1963) 702.
33) Y. Saito: J. Cryst. Growth 47 (1979) 61.
34) C. G. Granqvist and R. A. Bhrman: J. Appl. Rev. 47 (1976) 2200.
35) C. G. Granqvist and O. Hunderi: Phys. Rev. B 16 (1977) 3513.
36) P. A. Temple and C. E. Hathaway: Phys. Rev. B 7 (1973) 3685.
37) J. F. Morhange, G. Kanellis and M. Balkanski: Solid State Commun. 31 (1979) 805.
38) Z. Iqbal, A. P. Webb and S. Veprek: Appl. Phys. Lett. 36 (1980) 163.
39) T. Okada, T. Iwaki, H. Kasahara and K. Yamamoto: Jpn. J. Appl. Phys. 24 (1985) 161.
40) M. H. Brodsky, M. Cardona and J. J. Cuomo: Phys. Rev. B 16 (1977) 3556.
41) R. Alben, D. Weaire, J. E. Smith, Jr. and M. H. Brodsky: Phys. Rev. B 11 (1975) 2271.
42) G. Kanellis, J. F. Morhange and M. Balkanski: Phys. Rev. B 21 (1980) 1543.
43) H. Richter, Z. P. Wang and L.Ley: Solid State Commun. 39 (1981) 625.
44) S. Hayashi and H. Abe: Jpn. J. Appl. Phys. 23 (1984) L824.
45) S. Hayashi and K. Yamamoto: Superlattices and Microstructures 2 (1986) 581.
46) F. L. Galeener and G. Lucovsky: Phys. Rev. Lett. 37 (1976) 1474.
47) R. B. Laughlin and J. D. Joannopoulos: Phys. Rev. B 17 (1978) 4922.
48) C. A. Murray and T. J. Greytak: Phys. Rev. B 20 (1979) 3368.
49) F. L. Galeener and J. C. Mikkelsen, Jr.: Solid State Commun. 37 (1981) 719.

50) M. Balkanski, R. F. Wallis and E. Haro: Phys. Rev. B 28 (1983) 1928.

Chapter 3
Small Silicon Particles in Thin Films

3.1 Introduction

Raman spectroscopy is non-destructive and is one of the most useful techniques for characterizing the structures of amorphous materials.[1] In particular, amorphous and microcrystalline silicon (*a*- or μ *c*-Si) have been studies extensively by Raman scattering as a model for amorphous semiconductors. It is generally accepted that the Raman spectrum of *a*- or μ *c*-Si evolves from a broad spectrum around 480 cm^{-1} characteristic of an amorphous film to a single-line spectrum around 520 cm^{-1} characteristic of bulk silicon crystal (*c*-Si), depending on the crystallinity of the film. This feature has been reported for various films prepared by a variety of methods such as glow-discharge (GD),[2-7] sputtering[8-10] and chemical vapor deposition.[11,12] In these experiments, the above change in Raman spectrum has been utilized as a fast convenient method of determining whether the film is crystalline or amorphous.

It is noted that, however, the so-called amorphous spectrum does not necessarily mean a random network structure. We have indicated in Chapter 2 that the Si particles smaller than 100 Å show the amorphous-like Raman spectrum even though the particles are crystalline. On the basis of this observation, we extend our investigation to small Si particles in thin films.

First, we demonstrate that[13,14] Raman scattering measurement allows us to determine quantitatively the structural properties, especially the change in crystallinity, of so-called *a*-Si film prepared by the classical evaporation method. Evaporated Si films are used because of their simple nature,

which shows no complicated effects such as those expected to be produced by the GD technique, *e.g.* the effects of the incorporation of hydrogen and of the complex preparation conditions. Research into these films is thus expected to give a more detailed understanding of their structural properties. In fact, we will show in this chapter that the structural change of thermally-annealed *a*-Si films can be probed successfully by Raman scattering. Moreover, the energy of activation of the crystallization will be deduced from the volume fraction of crystallinity determined by resolving the spectrum.

Next, the Raman scattering measurement is applied to characterize GD-deposited Si film. We discuss the effects of preparation parameters on the structural properties with the aid of the volume fraction of crystallinity used for the evaporated Si film, as well as the linewidth of the Raman spectrum and the crystallite size calculated from X-ray diffraction. The results presented in this chapter show that the volume fraction of crystallinity characterizes quantitatively the structural change of μ *c*-Si film. In addition we consider the finite-size effects on the Raman spectra of GD-deposited μ *c*-Si comparing with the experiment on thermally annealed Si film reported in this chapter and the calculation made by Richter *et al.*[16]

3.2 Experimental

The silicon films used in the present experiments were prepared by vacuum evaporation; *c*-Si chips were evaporated from a boron-nitride boat in a vacuum of the order of 10^{-6} Torr. All deposits were made onto *c*-Si wafers at room temperature. Since the films were sufficiently thick (~ 10 μm), the substrates did

not affect the observed Raman spectra. The as-prepared wafers were split into small chips about 1 cm^2 in area, and these chips were used for a series of thermal annealing experiments.

The samples were placed in a quartz tube evacuated to a pressure of the order of 10^{-6} Torr, then inserted in an electric oven. The annealing temperature T_a of each run was maintained at a constant value within 2 %, and varied from 100 to 1000 °C. The annealing time was fixed at 30 minutes for all results reported here. The samples annealed at the desired temperature were quenched to room temperature in vacuum.

On the other hand, the μ c-Si films were deposited by RF plasma deposition from monosilane (SiH_4) diluted with hydrogen to 3 mol %. A capacitively coupled cross-field system with a RF oscillator of 4 MHz and DC electric field applied perpendicularly to the RF electric field was employed for the deposition of SiH_4. The RF power was varied from 40 to 300 W and DC bias voltage was controlled from - 50 to + 100 V, where the DC bias voltage was measured with respect to the substrate. The total gas flow rate was kept at 70 cc/min with a gas pressure of 0.9 Torr. The substrate of *n*-type crystalline Si was used and its temperature T_s was kept at 250, 300 and 350 °C. Using the above parameters, we get the μ c-Si films with about 1 μm in thick and the deposition rate of 0.24 - 6.17 Å/sec.

The crystallite size *d* of the μ c-Si film was evaluated from the width of (111) and (220) peaks of X-ray diffraction pattern using the Scherrer formula.

The Raman spectra of both the evaporated and GD-deposited silicon films were measured in a convenient 90° scattering configuration with about 50 mW of 4880 Å argon-ion laser radiation focused by a cylindrical lens at room temperature. The Raman

spectrometer was a SPEX RAMALOG 5M double monochromator with standard cooled photomultiplier and photon counting system. The Raman spectra were analyzed by a Du Pont 310 Curve Resolver; this approach is the same as used for the small Si particles in Chapter 2.

3.3 Structural Analysis of Evaporated Films

The results obtained by Raman scattering measurement of *a*- and μ *c*-Si have been interpreted in terms of changes in the TO-[2-4,7,8,17,18] and TA-like[18,19] phonon frequencies, the linewidth of the TO-like phonon band,[3,7,9-12,17,18] and the volume fraction of crystallinity.[5,6,20] These parameters have been correlated with a number of physical properties such as the electrical conductivity,[4-6,17,18,20] optical gap,[9] bond angle or dihedral angle distortion,[9,21] and density of dangling bonds.[10] In this section, we will discuss the structural change of the evaporated *a*-Si film in terms of the frequency and linewidth of the TO-like phonon mode and the volume fraction of crystallinity v_f of the film, limiting the frequency region to that corresponding to the TO band in *c*-Si.

Figure 3.1 shows a series of Raman spectra of evaporated Si films annealed at various temperatures. The spectrum of as-deposited film is a broad asymmetric hump around 480 cm^{-1} characteristic of so-called *a*-Si, while, for the films annealed at the annealing temperature T_a > 700 °C, a sharp structure slightly below 520 cm^{-1} dominates the spectra. These results clearly demonstrate the growth of the crystallites induced by the heat treatment.

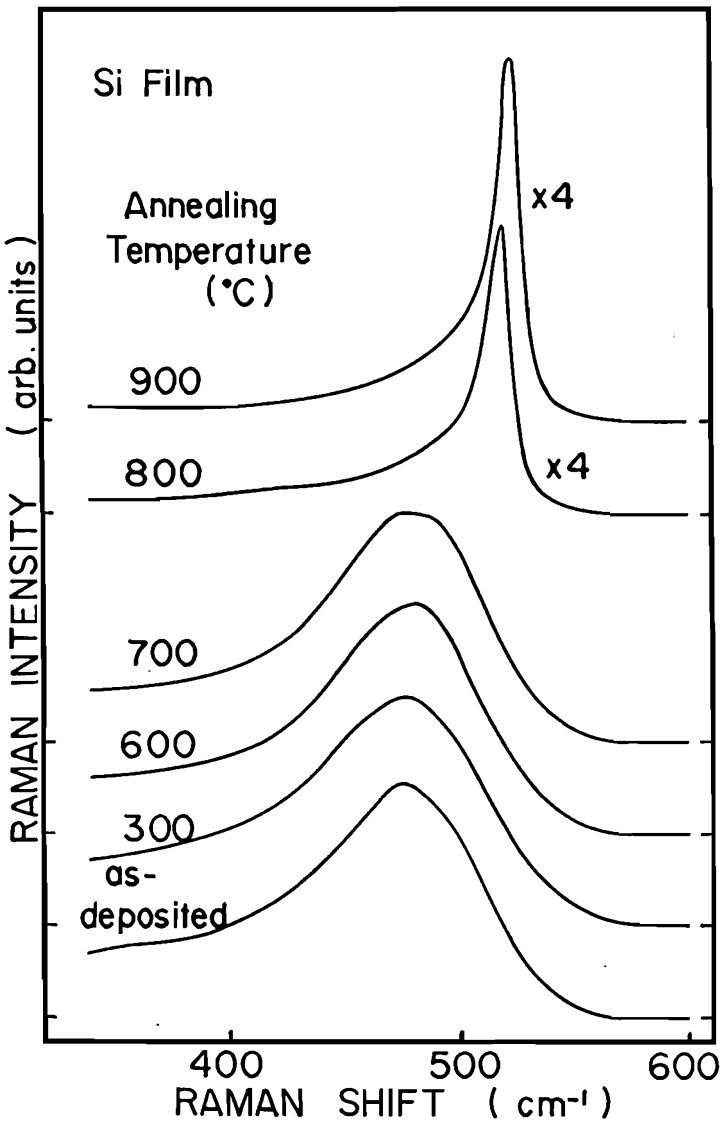

Fig. 3.1 A series of Raman spectra of evaporated silicon films annealed at various temperatures.

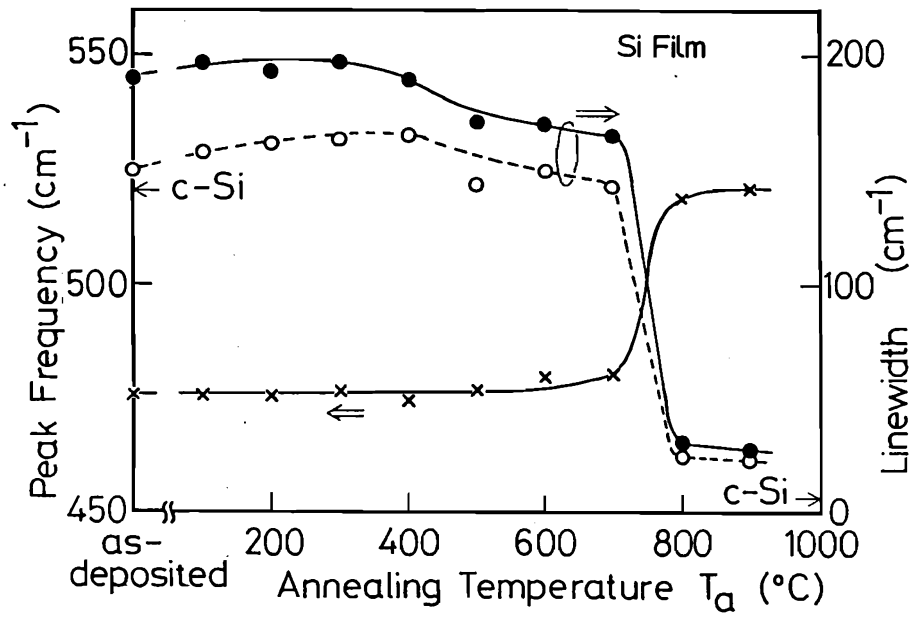

Fig. 3.2 Dependence of the peak frequency and linewidths of TO-like mode on the annealing temperature T_a. The linewidths are determined in two ways. (See details in the text.)

In Fig. 3.2, the apparent peak frequency and the linewidths of the TO-like mode are plotted as a function of T_a. The linewidths were determined in two ways; one was the usual full width at half maximum, assuming the zero level to correspond to the intensity at 600 cm^{-1} (closed circles), and the other was obtained by doubling the value measured from the peak to the half maximum on the high-frequency side (open circles). The latter has been used to avoid the contribution of the LO-like band

to the linewidth.[10,18] In the present result, however, the dependence of the two linewidths on T_a shows a very similar tendency, so it is difficult to discuss the contribution of the LO-like mode in this way.

The most prominent features observed in Fig. 3.2 are the abrupt changes in both the peak frequency and the linewidths just above 700 °C. This indicates that the large growth of crystallites takes place vigorously above this temperature. However, this temperature is not necessarily the unique temperature of crystallization, because its value depends strongly on the annealing conditions and is also affected by a complex effect of the TO- and LO-like modes. In fact, in samples subjected to preheat treatment at about 600 °C for 30 minutes, the abrupt changes were observed at a temperature 100 °C lower than that of the above case. Moreover, the following discussion using v_f will show that the structural change takes place at a constant rate from a considerably lower temperature.

Let us now consider v_f deduced from the Raman spectrum. To our knowledge, there are two methods of determining v_f from the measured Raman spectra[6,7,20] apart from analysis of polarized Raman scattering, which is suitable for quasi-single crystal silicon[22] but not for the present case. Mishima *et al.*[5,6] simply used the ratio of the peak height at 520 cm^{-1} to the height at 480 cm^{-1}, while Tsu *et al.*[20] used the integrated intensities of the resolved modes corresponding to the crystalline and amorphous-like parts. In the present discussion, we adopt a method similar to the latter, because it seems that the Raman peak heights used in the former do not correctly reflect the nature of the region probed by the laser beam.

Thus, the measured Raman spectra were resolved into several

components in the region from 250 to 600 cm^{-1}, assuming Gaussian lineshapes; this procedure is the same as used in § 2.4. Typical resolved modes are shown in Fig. 3.3. Although the resolved modes contain the LA- and LO-like modes similar to the small Si particles discussed in § 2.4, these are not the subject of the present discussion and are not shown in Fig. 3.3. When we obtain the integrated intensities of I_c and I_a as the crystalline component and the amorphous-like one, it is assumed that I_c and I_a represent the contributions from the ingredients of sufficiently large crystallites v_f and the remains composed of smaller crystallites $(1-v_f)$ in the probed volume. That is, they are given by

$$I_c = \Sigma_c v_f \quad \text{and} \quad I_a = \Sigma_a (1 - v_f), \tag{3.1}$$

where Σ is the integrated cross section over the resolved frequency range. Since I_c and I_a are measured on the same scale, even in arbitrary units, we can define v_f as

$$v_f = I_c / (I_c + \sigma_r I_a), \tag{3.2}$$

where σ_r is the ratio of the integrated Raman cross section for the crystalline to amorphous-like parts, Σ_c and Σ_a.

This procedure is similar to that of Tsu *et al.*[20] except that they attribute I_c to the area remaining under the curve after I_a has been subtracted from the total spectrum. We believe that our method of determining I_c and I_a is more appropriate because the values of I_c and I_a obtained are free from the contribution from the LO-like mode and accidental modes arising from impurities such as oxygen introduced during the deposition.

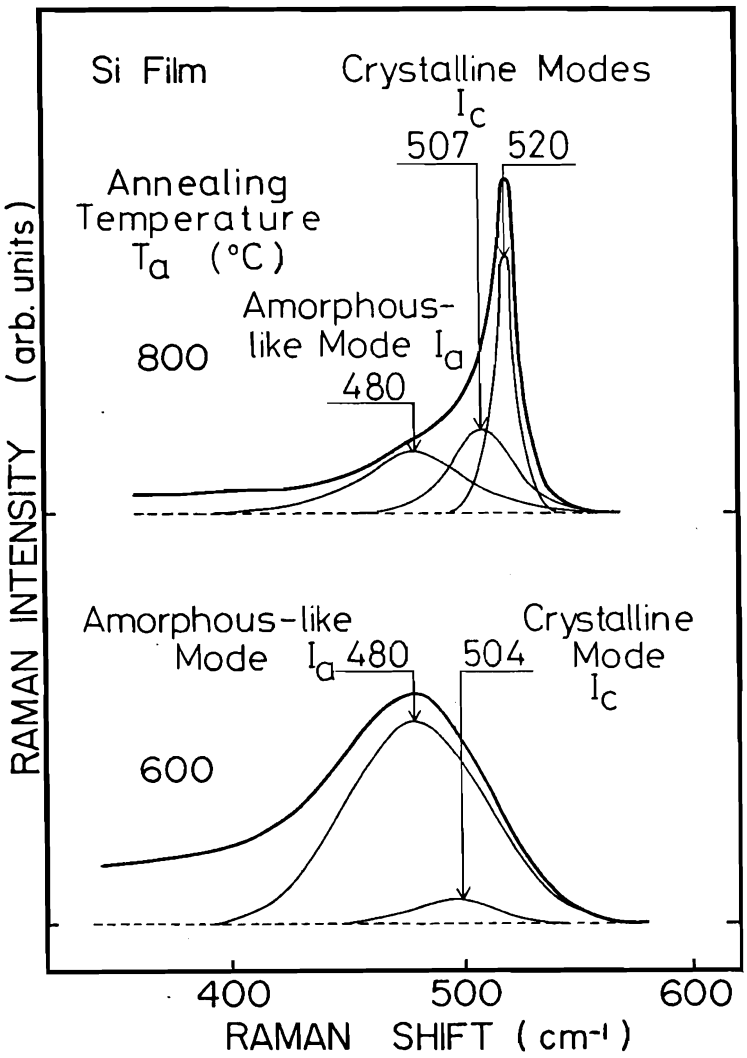

Fig. 3.3 Representative Raman spectra resolved into crystalline part(s) and amorphous-like part. The values indicated by the directed lines are peak frequencies in cm^{-1}.

To calculate v_f using eq. (3.2), we must estimate σ_r. The value of σ_r has been reported to be from about 0.1 for *a*-Si films relative to polycrystalline or single-crystal Si [23,24] to 0.88 for *a*-Si films relative to μ*c*-Si.[20] Obviously, the value of σ_r varies with various parameters such as the exciting photon energy and the crystallite size. However, we have used here a constant value of 0.8 as Tsu *et al.* have done.[20] This is reasonable because the optical properties of the crystalline and amorphous-like phases are similar in a coexistent film.

Then we discuss an analysis of the structural change of evaporated silicon film using v_f. The kinetics of the transformation of structure are commonly described by the Avrami formula.[25-27] For a process activated thermally with a single activation energy E_a at a fixed temperature T_a, which is exactly the present case, the Avrami formula becomes

$$1 - v_f = (1 - v_{f0}) \exp [- A \exp (- E_a / k_B T_a)], \qquad (3.3)$$

where v_{f0} is the initial value before the annealing and A is a constant under the present conditions.

Using eqs. (3.2) and (3.3), we give the Arrhenius plots of $\ln [(1 - v_{f0}) / (1 - v_f)]$ in Fig. 3.4, where the two sample sets are used. The closed circles and the crosses denote, respectively, non-heat-treated films (the same as those in Fig. 3.1) and films pre-heat-treated at about 600 °C for 30 minutes before the regular annealing. In spite of the different value of v_{f0} (v_{f0} = 0 or 0.16), the structural change of two sample sets obeys the same equation, eq. (3.3).

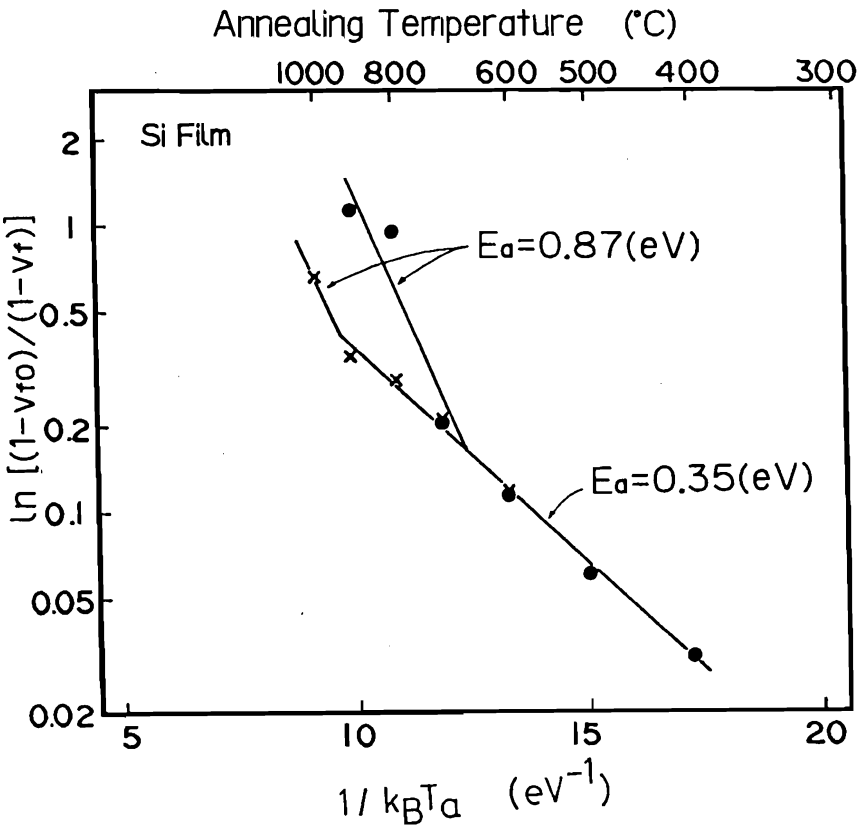

Fig. 3.4 Arrhenius plots of ln [(1 - v_{f0}) / (1 - v_f)] versus inverse temperature, where v_{f0} and v_f are values before and after annealing. The circles and crosses designate sample sets without and with preheat treatment, respectively. The solid lines are least-squares fits to the experimental points. Also, the activation energy E_a is the slope of the above solid lines.

It is evident that the evaporated Si films are crystallized

in two stages with E_a = 0.35 and 0.87 eV in our measurement range. The value of E_a is the slope determined by a least-squares fit to the experimental points. It is pointed out for the first time that the structural change continues from T_a < 400 °C at a constant rate. In addition, we postulate that the E_a of 0.35 eV is identical to the activation energy for the viscous flow of Si, 0.37 eV (8.63 kcal/mol).[28]

The activation energy for the crystallization of *a*-Si has been determined by different measurement techniques (*e.g.* Raman scattering,[25] X-ray diffraction,[27] optical transmission,[29] and conductivity measurement[30]) for various preparation methods (*e.g.* sputtering,[25] GD,[20] chemical vapor deposition,[27] and evaporation[29,30]). These values lie in the range from 0.8 to 4.9 eV, and several interpretations of the large scatter have been found in the literature.[25,27,29,30] However, these cannot fully explain the present result. Our interpretation will be given in Chapter 5 in connection with the result of germanium particles and films.

3.4 Structural Analysis of Glow-Discharge Deposited Films

In this section, we consider the structural properties of GD-deposited silicon films by using the volume fraction of crystallinity v_f, which is the same as defined in § 3.3, the linewidth (full width at half maximum) of Raman peak Γ, and the crystallite size d. A example of the Raman spectrum and its resolved modes is shown in Fig. 3.5, in which the preparation conditions are given. Our main purpose is to discuss the effect of preparation conditions on the crystallinity of the films.

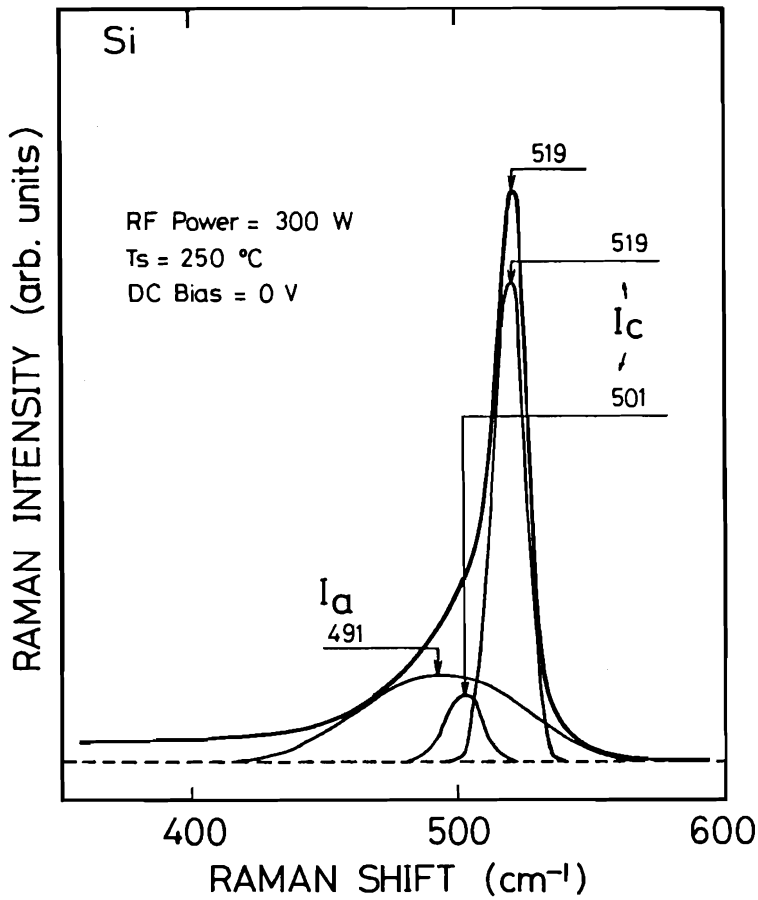

Fig. 3.5 A example of the Raman spectrum and its resolved modes of GD-deposited silicon films. I_c and I_a are the integrated intensities of the crystalline and amorphous-like components. The values indicated by directed lines are peak frequencies in cm^{-1}

First, the dependence of v_f, Γ and d on the RF power is shown in Fig. 3.6. As the power increases, the increase of the crystallinity is observed. In particular, v_f has a linear correlation with the power. In contrast to v_f, d and Γ indicate more complicated behavior: d has the maximum around 180 W and then decreases gradually; simultaneously, Γ decreases first and then the minimum at that power and then increase. The change at the power below and above 180 W are probably caused by, respectively, the increase of smaller crystallites, and the stress formed in the film as well as the finite-size effects discussed in detail later.

It is instructive to compare the above results with those reported by Mishima *et al.*,[5] because they have clearly described the effect of RF power on the crystallite formed in GD-deposited μc-Si. They have conclude that the volume fraction of crystallinity increases with increasing the power, and that this increase arises from the increase of the number of crystallites without any accompanying change in the crystallite size. The former conclusion agrees with ours in spite of the different method of determination of v_f; the latter, however, disagrees with ours. We feel that the constant value of d is a oversimplified assumption. The result reported here indicates the variation of d with the power. Moreover, the films deposited at above 180 W show the decrease of d but the increase of v_f. Thus we conclude with the aid of v_f that the dense films with the crystallites are deposited at high power.

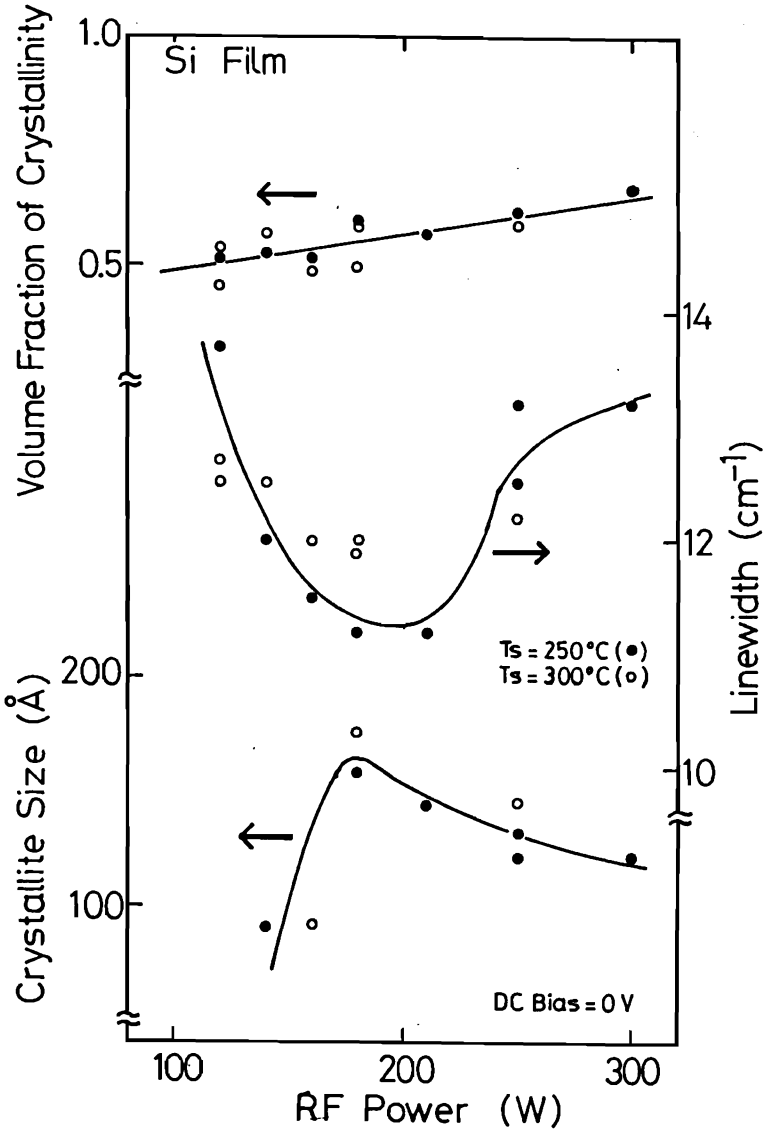

Fig. 3.6 The volume fraction of crystallinity v_f, the linewidth of Raman peak Γ, and the crystallite size d as a function of the RF power.

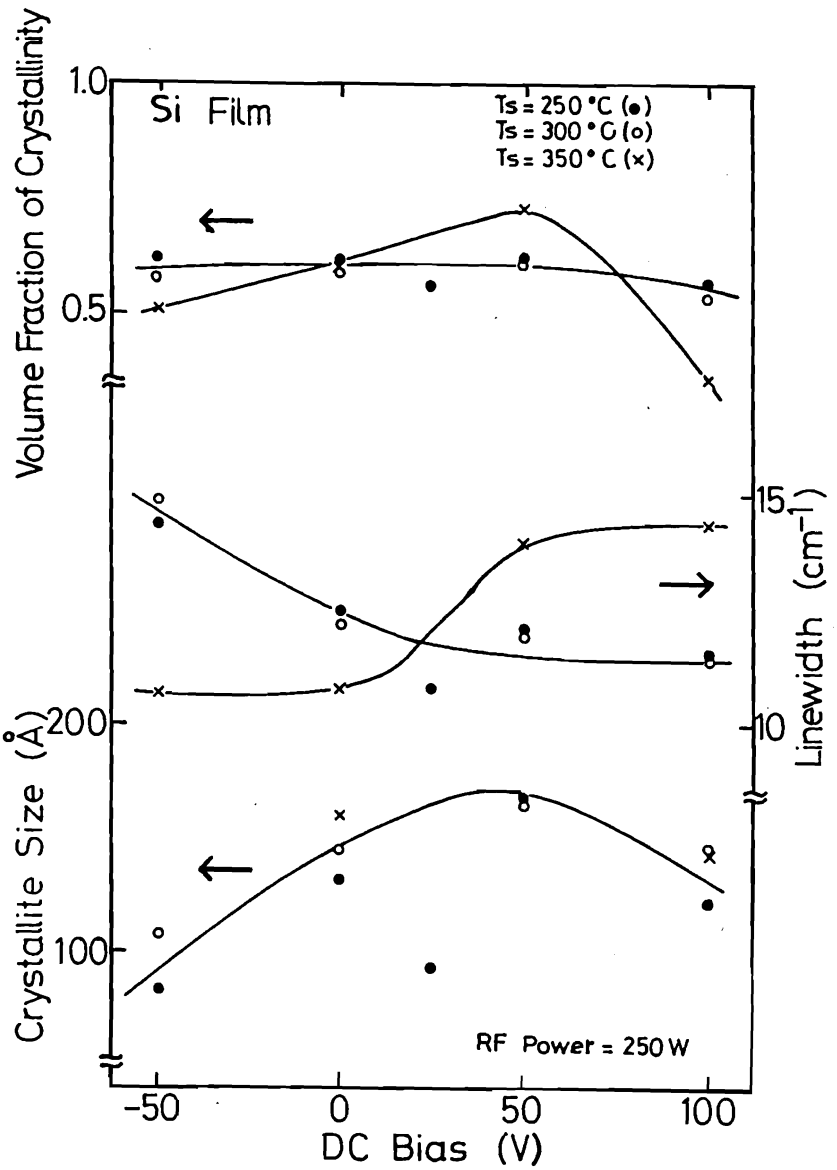

Fig. 3.7 The volume fraction of crystallinity v_f, the linewidth of Raman peak Γ, and the crystallite size d as a function of the DC bias voltage.

Second, v_f, Γ and d are plotted as a function of the DC bias voltage V_b in Fig. 3.7. The observed features in this figure are as follows: (1) v_fs in the films deposited at the substrate temperature T_s = 250 and 300 °C are nearly constant in our experimental condition, but v_fs in the films deposited at T_s = 350 °C have the maximum value around 50 V and are degraded by the positive V_b higher than 50 V. (2) The films deposited at T_s = 250 and 300 °C are very different from those deposited at T_s = 350 °C in the V_b dependence of Γ ; Γ s of the former films decease with the change in V_b from - 50 to 100 V, but Γ s of the latter films increase with the same change. (3) In contrast to v_f and Γ , ds are independent of T_s; they have maximum around 50 V.

Several groups have reported the effect of DC bias on the structural properties.[31-35] From the comparison of the results reported previously with ours, we suggest the following interpretation: In the condition of negative V_b, the growing surface is subject to the bombardment of positively charged radicals. Therefore the increase in Γ of the film deposited at T_s = 250 or 300 °C comes from the stress induced by the bombardment during the growth, although the higher T_s (350 °C) relaxes this stress. On the other hand, the positive bias promotes the growth of crystallite up to about 50 V. This tendency agrees with the results reported by Matsuda *et al.*[35] However the decrease of d at V_b higher than 50 V disagrees; this is attributable, at least in part, to the different method applying DC bias voltage. Finally, we consider that the V_b dependence of v_f and Γ is different from T_s's (the above (1) and (2)). It seems that SiH_x radicals are related to this difference. Since the higher T_s enhances the surface mobility of diffusing radi-

cals,[31,35] it may relax the stress; or, since the first hydrogen evolution takes place at above 300 °C,[36,37] it may hinder from growing the crystallite. These contrary effects make the experimental results intricate, and the further study is needed for full clarification of the formation kinetics.

At last, a comparison of our experimental results with several theoretical calculations is made on the first order Raman mode observed in silicon films. The formation of large microcrystals in Si films gives rise to the sharp crystalline mode, which more or less accompanies the frequency shift and broadening. Several attempts to estimate the finite-size effects of microcrystals on this spectral change have been reported in terms of a continuous-random-network structure,[10] a very simple valence-force-field model for two-dimensional Si thin slab,[38] and a relaxation of the wave-vector selection rule.[7,16,39]

The calculation model proposed by Richter *et al.*[16] is the most suitable for comparing our results because of their simple but valuable results. In their model, the localization due to the relaxation of the conservation of crystal momentum in microcrystal has been described by a new wave function ψ in the form

$$\psi(q_0,r) = A \exp\left[-\left(\frac{r^2}{2}\right)\Big/\left(\frac{L}{2}\right) - iq_0\cdot r\right] u(q_0\cdot r), \quad (3.4)$$

where q_0 is the phonon wave vector, L is the diameter of the spherical crystallite, and $u(q_0\cdot r)$ has the periodicity of the lattice. The quantity ψ is no longer the eigenfunction of q_0, so it leads to a broadening of the Raman-active line and a con-

comitant red shift of its mean position. Richter *et al.*'s result is shown by the solid line in Fig. 3.8. In this figure, our results of the evaporated and the GD-deposited Si films are plotted by open and closed circles respectively.

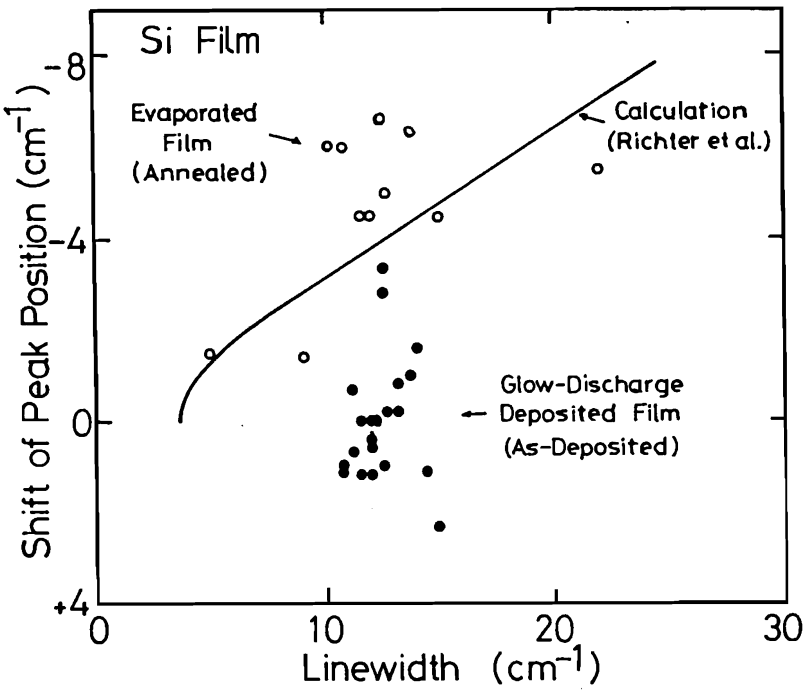

Fig. 3.8 Comparison between the experimental data (closed and open circles) and the calculated line made by Richter *et al.*[16] (solid line). The closed and open circles denote, respectively, the GD-deposited Si film and the evaporated Si film annealed thermally.

In spite of the great simplification involved, the relation between the shift of peak position and the linewidth for evaporated film annealed thermally is explained fairly well by the simple model. However, this is not the case in the relation for the GD-deposited film; all the points obtained appear on the high frequency side of the calculated line. This is probably caused by the effect of stress. The shift to higher frequency suggests a compressive stress.[40] In addition, we can estimate the stress to be several kbar, which is the same order of the other estimation.[33,41] The above result shows that the relaxation of the wave-vector selection rule is effective for the interpretation of finite-size effect of the microcrystals in film. But it must be noted that the finite-size effects of the small particles with free boundary condition are not explained by the relaxation of the wave-vector selection rule only. The amorphous-like broad spectrum of small Si particles with crystalline structure discussed in § 2.4 is not interpreted by this model. Although some mechanisms are proposed,[42,43] further experimental and theoretical investigations are required.

3.5 Summary

Evaporated silicon films annealed thermally at various temperatures were studied by Raman scattering. The Raman spectra were analyzed in terms of the peak frequency and the linewidths for the TO-like mode together with the volume fraction of crystallinity v_f determined from the integrated intensities of resolved modes corresponding to the crystalline part and the amorphous-like one. Moreover, by fitting v_f to the Avrami formula, we found the two different activation energy for the structural change. The very low activation energy of 0.35 eV was

determined and found to be the activation energy for viscous flow of Si.

The Raman scattering study was extended to GD-deposited Si films. The dependence of preparation parameters of the RF power and the DC bias voltage on the structural properties was discussed by using v_f, the linewidth of the Raman spectrum, and the crystallite size determined from X-ray diffraction. In order to interpret the finite-size effect of small particle formed in film, we compared our experimental results of evaporated and GD-deposited films with the theoretical calculation made by Richter *et al.*; which is based on the relaxation of the wave-vector selection rule. We suggested that further study is needed to clarify the finite-size effects for the small particles.

References

1) For example, M. H. Brodsky and M. Cardona: J. Non-Cryst. Solids 31 (1981) 81.

2) Z. Iqbal, A. P. Webb and S. Veprek: Appl. Phys. Lett. 36 (1980) 163.

3) Z. Iqbal, S. Veprek, A. P. Webb and P. Capezzuto: Solid State Commun. 37 (1981) 993.

4) T. Kamiya, M. Kishi, A. Ushirokawa and T. Katoda: Appl. Phys. Lett. 38 (1981) 377.

5) Y. Mishima, T. Hamasaki, H. Kurata, M. Hirose and Y. Osaka: Jpn. J. Appl. Phys. 20 (1981) L121.

6) Y. Mishima, S. Miyazaki, M. Hirose and Y. Osaka: Philos. Mag. B 46 (1982) 1.

7) Z. Iqbal and S. Veprek: J. Phys. C: Solid State Phys. 15 (1982) 377.

8) T. Imura, K. Mogi, A. Hiraki, S. Nakashima and A. Mitsuishi: Solid State Commun. 40 (1981) 161.

9) J. S. Lannin, L. J. Pilone, S. T. Kshiragar, R. Messier and R. C. Ross: Phys. Rev. B 26 (1982) 3506.

10) A. Morimoto, M. Kumeda and T. Shimizu: J. Non-Cryst. Solids 59 & 60 (1983) 537.

11) S. T. Kshirsagar and J. S. Lannin: Phys. Rev. B 25 (1982) 2916.

12) E. Bustarret, A. Deneuville, H. R.-Buisson and L. Brunel: J. Non-Cryst. Solids 59 & 60 (1983) 205.

13) T. Okada, T. Iwaki, H. Kasahara and K. Yamamoto: Solid State Commun. 52 (1984) 363.

14) T. Okada, T. Iwaki, H. Kasahara and K. Yamamoto: Jpn. J. Appl. Phys. 24 (1985) 161.

15) T. Okada and K. Yamamoto: IECEJ Tech. Rep. SSD84-158 (1985-

3) 75 [in Japanese].
16) H. Richter, Z. P. Wang and L.Ley: Solid State Commun. 39 (1981) 625.
17) S. Nakashima, S. Oima, A. Mitsuishi, T. Nishimura, T. Fukumoto and Y. Akasaka: Solid State Commun. 40 (1981) 765.
18) R. Tsu, J. G.-Hernandez, J. Doehler and S. R. Ovshinsky: Solid State Commun. 46 (1983) 79.
19) T. Shimada, Y. Katayama, K. Nakagawa, H. Matsubara, M. Migitaka and E. Maruyama: J. Non-Cryst. Solids 59 & 60 (1983) 783.
20) R. Tsu, J. G.-Hernandez, S. S. Chao, S. C. Lee and K. Tanaka: Appl. Phys. Lett. 40 (1982) 534.
21) R. Tsu, J. G.-Hernandez and F. H. Pollak: Solid State Commun. 54 (1985) 447.
22) M. Nakamura, Y. Kobayashi and K. Usami: Jpn. J. Appl. Phys. 23 (1984) 687.
23) M. H. Brodsky, M. Cardona and J. J. Cuomo: Phys. Rev. B 16 (1977) 3556.
24) D. Bermejo and M. Cardona: J. Non-Cryst. Solids 32 (1979) 405.
25) J. G.-Hernandez and R. Tsu: Appl. Phys. Lett. 42 (1983) 90.
26) J. W. Christian: *The Theory of Transformations in Metals and Alloys* (Pergamon Press, London, 1965).
27) M. Janai, D. D. Allred, D. C. Booth and B. O. Seraohin: Sol. Energy Mater. 1 (1979) 11.
28) A. J. Moses: *The Practicing Scientist's Handbook* (Van Nostrand Reinhold, New York, 1978) p.1021.
29) N. A. Blum and C. Feldman: J. Non-Cryst. Solids 11 (1972) 242.
30) K. Zellama, P. Germain, S. Squelard, J. C. Bourgoin and P.

A. Thomas: J. Appl. Phys. 50 (1979) 6995.

31) J. C. Knights and R. A. Lujan: Appl. Phys. Lett. 35 (1979) 244.

32) H. Okamoto, T. Yamaguchi, T. Nitta and Y. Hamakawa: J. Non-Cryst. Solids 35 & 36 (1980) 201.

33) F.-A. Sarott, Z. Iqbal and S. Veprek: Solid State Commun. 42 (1982) 465.

34) A. Matsuda: J. Non-Cryst. Solids 59 & 60 (1983) 767.

35) A. Matsuda, K. Kumagai and K. Tanaka: Jpn. J. Appl. Phys. 22 (1983) L34.

36) M. H. Brodsky, M. A. Frisch, J. F. Ziegler and W. A. Lanford: Appl. Phys. Lett. 30 (1977) 561.

37) S. Oguz, R. W. Collins, M. A. Paesler and W. Paul: J. Non-Cryst. Solids 35 & 36 (1980) 231.

38) G. Kanellis, J. F. Morhange and M. Balkanski: Phys. Rev. B 21 (1980) 1543.

39) I. H. Campbell and P. M. Fauchet: Solid State Commun. 58 (1986) 739.

40) B. A. Weinstein and G. J. Piermarini: Phys. Rev. B 12 (1975) 1172.

41) T. Iwaoka, S. Yokoyama and Y. Osaka: Jpn. J. Appl. Phys. 24 (1985) 112.

42) S. Hayashi and H. Abe: Jpn. J. Appl. Phys. 23 (1984) L824.

43) S. Hayashi and K. Yamamoto: Superlattices and Microstructures 2 (1986) 581.

Chapter 4
Raman Depolarization Analysis of Small Silicon Particles

4.1 Introduction

It is well-known that the structure of the Raman tensor can be determined from the Raman polarization analysis of an oriented single crystal. On the other hand, the symmetry character of vibrational modes for randomly oriented samples such as small particles and fluid systems are characterized by a depolarization ratio ρ defined as the ratio of the depolarized to the polarized Raman intensities. In any case the polarization properties of the Raman spectrum of a material provide us with the symmetry character for Raman-active modes.

Thus we discuss in this chapter the Raman polarization measurement of small silicon particles[1] following our previous Raman scattering study of the same substance; in the previous study described in Chapters 2 and 3 we did not pay much attention to the polarization properties. The motivation of this work is twofold: to investigate finite-size effects on the vibrational modes from the point of view of the symmetry properties and to contribute to the study of the structure of amorphous silicon. The dependence of the depolarization ratio ρ for the Si particles on the particle size is reported for the first time. Then the results are discussed by analogy with liquids and gases[2] and compared with the results of amorphous Si reported previously.[3-6]

4.2 Experimental

The small Si particles were prepared by the gas-evaporation

technique. Details of the experiments are the same as given in § 2.2. By varying the argon gas pressure from 0.1 to 1 Torr, we obtained the Si particles 60 to 350 Å in the average particle size d. The size ds were determined from electron micrographs obtained by a Hitachi HS-7D electron microscope.

The Raman measurements were made by the same apparatus as used in § 2.2. To analyze the polarization properties, we recorded Raman spectra with two different Raman polarization configurations using the right-angle scattering geometry. That is, the scattering intensities of depolarized (I_V) and polarized (I_H) spectra were obtained at the $X(ZX)Y$ and $X(ZZ)Y$ geometries respectively, where X axis is taken for the direction of laser beam with its electric vector in the Z direction and Y axis for the direction of scattered light. Thus we can define the depolarization ratio ρ as I_V/I_H. The measured values of ρ were calibrated against reference peaks of carbon tetrachloride, whose 218- and 314-cm^{-1} lines are known to be completely depolarized ($\rho = 0.75$).

4.3 Discussion of Raman Depolarization Ratio

The polarized (I_H) and depolarized (I_V) Raman spectra for the particles 350 and 60 Å in size are shown in Fig. 4.1. For particles smaller than about 100 Å, the polarized and depolarized spectra show a broad amorphous-like band. For large particles, the spectra consist of a sharp crystalline peak and a broad amorphous-like band. The size dependence of the polarized and depolarized spectra presently observed is similar to that of un-polarized spectra previously observed (see § 2.4).

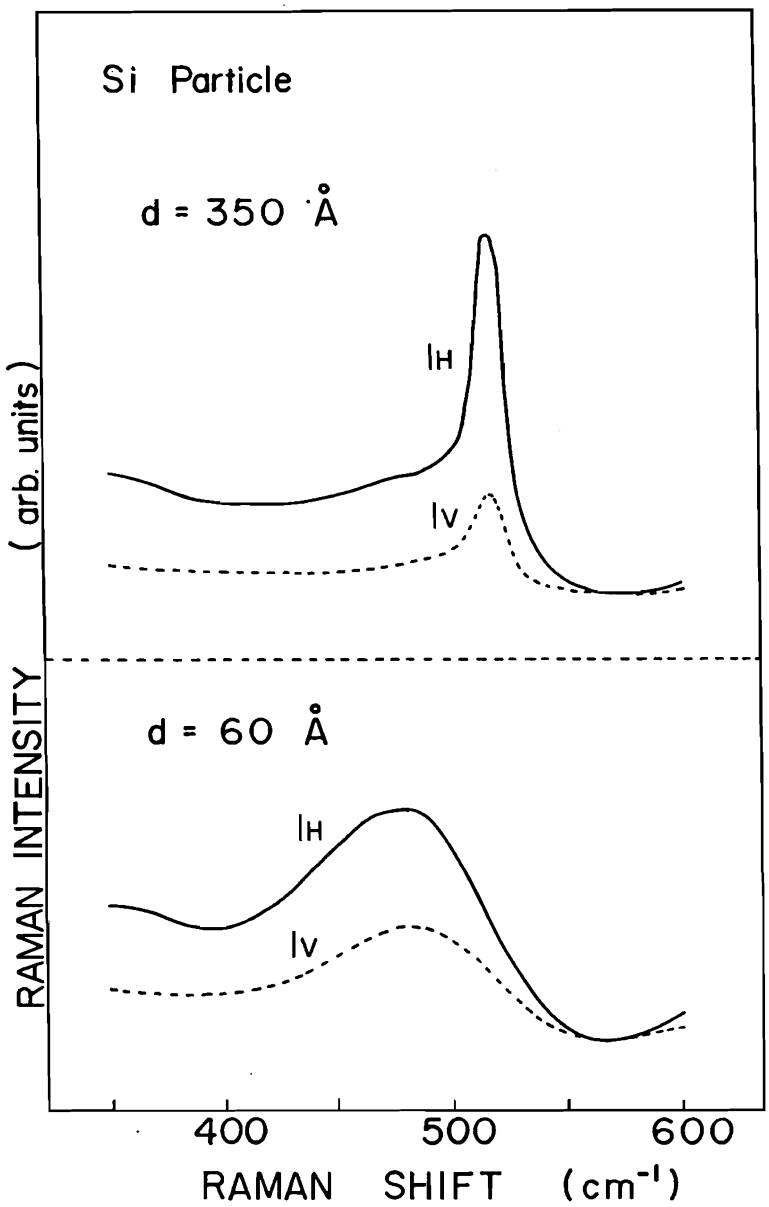

Fig. 4.1 Depolarized (I_V) and polarized (I_H) Raman spectra of the small silicon particles 350 and 60 Å in the average particle size d.

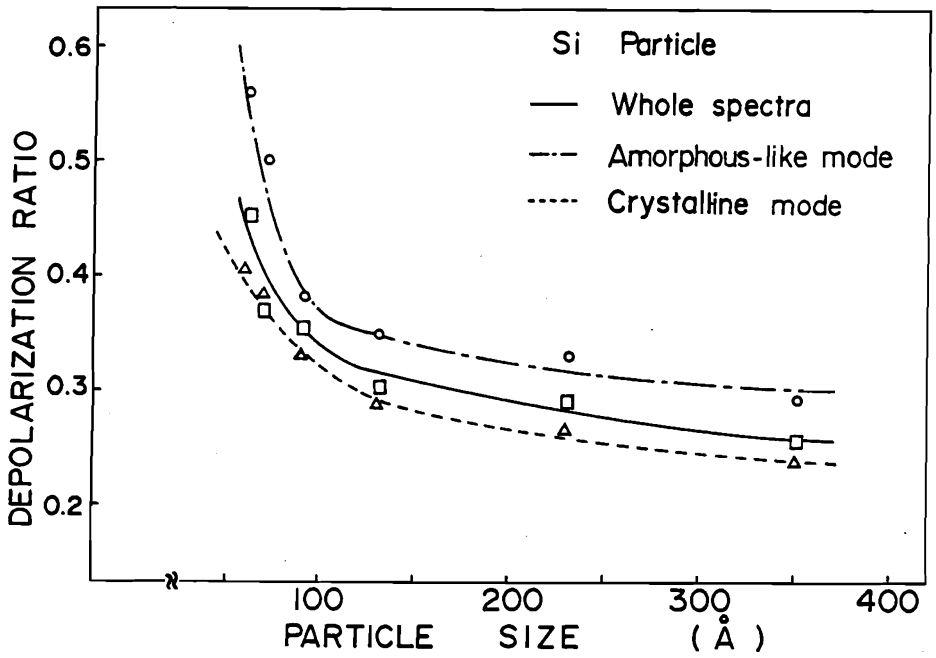

Fig. 4.2 Depolarization ratio ρ of the small silicon particles as a function of the average particle size d. There are three ρ s determined from the whole spectrum (a solid line), the crystalline mode (a broken line), and the amorphous-like mode (a dash-dotted line).

To obtain the depolarization ratio ρ , we first integrated the polarized and depolarized intensities over the whole spectral range studied and then took the ratio. Furthermore, since the spectra consist of several modes, we also obtained the depolarization ratio ρ for each component. To do so, the

spectra were decomposed into the components by the same resolving procedure used for un-polarized spectra (see § 2.2). Then the ratios were calculated from the integrated intensities of two resolved modes, the amorphous-like mode ($\sim$ 480 cm^{-1}) and the crystalline mode ($\sim$ 520 cm^{-1}).

The obtained values of ρ s are shown in Fig. 4.2 as a function of d. The ρ of whole spectrum decreases from 0.45 at d = 60 Å to 0.25 at d = 350 Å. The ρ s of amorphous-like and crystalline modes are slightly larger and smaller than the ρ of whole spectrum, respectively, in the size range of Fig. 4.2. The spectrum of the particles with smaller size is dominated by the amorphous-like mode, thus ρ of the amorphous-like mode becomes accurate for smaller size. In contrast, since the spectrum for larger size is dominated by the crystalline mode, an error in ρ of crystalline mode is small for larger size. Thus we discuss the implication of ρ s by separating the region into two, the regions of size smaller and larger than about 100 Å.

First, we discuss the result of ρ of crystalline mode, i.e. mainly the region of larger size. As reported previously,[1,2,8] the gas-evaporated Si particles possess the crystalline structure. We thus regard the present system as an assembly of the particles with the same Raman tensors as those of the bulk Si. By analogy with liquids and gases,[3] ρ for the randomly oriented particles is given by

$$\rho = \frac{I_V}{I_H} = \frac{3\beta^2}{45\alpha^2 + 4\beta^2}, \qquad (4.1)$$

where

$$\alpha = \frac{1}{3}(\alpha_{xx} + \alpha_{yy} + \alpha_{zz}), \tag{4.2}$$

$$\beta^2 = \frac{1}{2}[(\alpha_{xx} - \alpha_{yy})^2 + (\alpha_{yy} - \alpha_{zz})^2 + (\alpha_{zz} - \alpha_{xx})^2$$

$$+ 6(\alpha_{xy}^2 + \alpha_{yz}^2 + \alpha_{zx}^2)], \tag{4.3}$$

and α_{ij} is the component of Raman tensors; α^2 and β^2 are the isotropic and anisotropic parts of the tensor, respectively.

In the present system we can predict $\rho = 3/4$, because all the diagonal components of the Raman tensors for the phonon of F_{2g} symmetry in Si crystal are zero. However the experimental values are much lower than the predicted value. We believe that this disagreement implies that the phonon in the Si particles has no more the F_{2g} symmetry. For the gas-evaporated Si particles smaller than several hundred angstrom, bulk concepts such as the F_{2g} symmetry and k-selection rule are thought to be inoperative. If it is so, ρ should increase to the ideal depolarization limit of 0.75 as the particle size increases. To check this, we made a preliminary experiment. Relatively large particles ($\sim$ 1000 Å) prepared by grinding the bulk Si show ρ = 0.89. This result indicates that the large particles can be regarded as small crystals with the F_{2g} symmetry. However, it may be considered that the higher value than the ideal depolarization limit for a plane polarized incident light

results from a natural (un-polarized) incident light induced by a multiple scattering; the natural light leads $\rho \rightarrow 6/7$.[3] To elucidate the size effects of polarization property, further experiments concerning the size range $d > 350$ Å are necessary. It is noted, however, that the preliminary experiment showed some difficulty in making stably the Si particles much larger size; this difficulty is probably caused by a decomposition of a boron nitride boat at high evaporation temperature.

We now consider the region dominated by the amorphous-like mode. For this region, ρ ranges around 0.5, which agrees with values of amorphous or microcrystalline Si films prepared by various methods.[4-7] In comparing our result with those of Si films, we are interested in the relationship between the structures and the polarization properties. Kobliska and Solin[9] suggested that the polarization properties of the Raman spectra can be used to test the validity of two structural models of amorphous materials, a random network model and a molecular one. On the basis of their results, Iqbal and Vepřek[7] have summarized the properties of ρ as follows: In a continuous random network (CRN) model, ρ should be frequency-dependent because all vibrational modes with different local symmetry characters contribute to the scattering. In contrast, molecular-like clusters show $\rho \rightarrow 0$ in the ideal case of no intercluster interaction but higher value in the condensed case.

The frequency dependence of ρ of the particles with 60 Å in d shows a featureless frequency-independent value of about 0.4, as plotted in Fig. 4.3. Figure 4.3 also includes the result for ρ of our evaporated Si film, which has been considered to have a typical amorphous structure. These values of the particles and films are the same within an experimental error. As

mentioned above, if so-called amorphous Si is CRN, ρ should show frequency-dependent feature. However the present results are contrary to the prediction of the CRN model. Therefore, the CRN model is inadequate to describe the structures of the Si particles and films showing broad amorphous-like Raman spectra. In addition, the molecular-like cluster model do not explain fully the present results, *e.g.* an increasing tendency of ρ with decreasing d, and the same values for the particles and films. We thus suggest that neither the CRN model nor the molecular-like model explains the structures of materials showing amorphous-like Raman spectra.

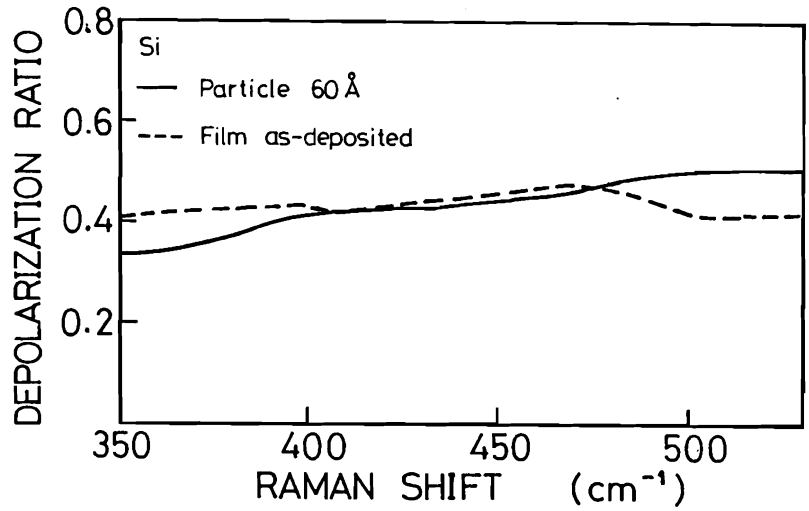

Fig. 4.3 Frequency dependence of the depolarization ratio ρ s of the small silicon particles 60 Å in the average particle size (a solid line) and of evaporated silicon film (a broken line).

According to the observation of high resolution electron microscopy,[8,10] it is apparent that both the particles and films consist of microcrystals. The agreement between the results of particles and those of films indicates that the structures in both systems must essentially be identical at least in Raman scattering process. We thus believe that the microcrystalline model is appropriate to describe the structures of the Si particles and films. However the reason why small crystalline particles exhibit the amorphous-like spectra is uncertain at present. Hayashi and Yamamoto[11] reported an attempt to interpret the amorphous-like signal as an enhanced signal from the surface layer of microcrystals. Theoretical investigations properly treating intrinsic surface effects are required.

4.4 Summary

We reported for the first time the Raman depolarization ratio ρ of small silicon particles with an average particle size from 60 to 350 Å. The low values of ρ for the particles having a crystalline peak were not explained by regarding the particles as the bulk Si. Thus bulk concepts such as the F_{2g} symmetry and k-selection rule were inoperative to the small Si particles. By comparing ρs of the Si particles with those of Si films, we have showed that the broad amorphous-like spectra do not mean the continuous random network structure or molecular-like cluster. The experimental results presented here were not predicted by existing theories. To discuss the finite-size effects observed here, lattice-dynamical calculations of Raman scattering are strongly needed.

References

1) T. Okada, T. Iwaki, K. Yamamoto, H. Kasahara and K. Abe: Solid State Commun. 49 (1984) 809.

2) T. Okada, T. Iwaki, H. Kasahara and K. Yamamoto: J. Phys. Soc. Jpn. 54 (1985) 1173.

3) T. R. Gilson and P. J. Hendra, *Laser Raman Spectroscopy* (Wiley-Interscience, London, 1970).

4) J. E. Smith, Jr., M. H. Brodsky, B. L. Croeder, M. Z. Nathan and A. Pinczuk: Phys. Rev. Lett. 26 (1971) 642.

5) D. Bermejo and M. Cardona: J. Non-Cryst. Solids 32 (1979) 405.

6) C. C. Tsai and R. J. Nemanich: J. Non-Cryst. Solids 35 & 36 (1980) 1203.

7) Z. Iqbal and S. Veprek, J. Phys. C: Solid State Phys. 15 (1982) 377.

8) S. Hayashi and H. Abe: Jpn. J. Appl. Phys. 23 (1984) L824.

9) R. J. Kobliska and S. A. Solin: Phys. Rev. B 8 (1973) 756.

10) For example, Y. Saito: J. Phys. Soc. Jpn. 53 (1984) 4230.

11) S. Hayashi and K. Yamamoto: Superlattices and Microstructures 2 (1986) 581.

Chapter 5
Small Germanium Particles

5.1 Introduction

The elements of Si and Ge belong to the same group IV and have similar properties. For example, Raman spectra of so-called amorphous and microcrystalline films usually exhibit two components, a sharp one called crystalline component, which resembles a sharp peak observed in bulk crystals (located at 520 cm^{-1} for Si and 300 cm^{-1} for Ge), and a broad one called amorphous-like component, which resembles a broad peak observed in so-called amorphous films (located at $\sim$ 480 cm^{-1} for *a*-Si and $\sim$ 280 cm^{-1} for *a*-Ge). So it is informative to expand our investigation on the small particles of Si to those of Ge by using the same method.

The size dependence of Raman spectra from small Ge particles with free boundary conditions has been reported by Hayashi *et al.*[1] They demonstrated that the Raman spectrum of the Ge particles as small as 80 Å shows the broad amorphous-like feature; this is consistent with the result of the small Si particles discussed in Chapter 2. We also observed the similar size dependence of Raman spectra from gas-evaporated Ge particles.

Although the size dependence is interesting, we focus our attention, in this chapter, on the structural changes of small Ge particles both with free boundary conditions and in thin film. By using the same analytical method as used for the Si particles, two-step structural change of the Ge particles and films is detected for the first time. On the basis of microcrystalline model, the mechanisms of this two-step change are dis-

cussed in relation to the result of the Si particles. We suggest that the low activation energy of incipient stage arises from the ordering of surface atoms of microcrystals,[2] and the later high energy results from the coalescence of microcrystals.[3]

5.2 Experimental

Germanium films were deposited by vacuum evaporation of Ge single crystal (purity 9N %) onto crystalline Si wafers at room temperature. The films were subsequently annealed in a vacuum of the order of 10^{-6} Torr at a fixed annealing temperature T_a from 250 to 600 °C for 20 or 30 minutes.

Small Ge particles were also deposited onto crystalline Si wafers by evaporating bulk Ge from a tungsten boat in Ar gas of 0.75 Torr (gas-evaporation). The Ge particles collected were then thermally annealed in the same vacuum condition as used for the film for 20 min. The annealing temperature T_a was varied from 200 to 500 °C with a step 50 °C.

Raman scattering from the as-deposited and annealed samples of particles and films was measured by a SPEX RAMALOG 5M spectrophotometer equipped with a double monochromator and a photon counting system. The 4880- or 5145-Å line of an Ar-ion laser was used to excite the spectra; to avoid the local heating of the samples of small particles, the laser power at sample points was kept less than 10 mW. The Raman spectra measured were resolved into crystalline mode ($\sim$ 300 cm^{-1}) and amorphous-like one ($\sim$ 280 cm^{-1}). The resolving was carried out on a microcomputer (Fujitsu FM-8) by assuming Gaussian lineshapes.

After completing the Raman measurements, the Ge particles

were scraped off from the substrate and dispersed in ethyl alcohol. A drop of the alcohol was put on a standard electron microscopic grid covered with a thin carbon film. After the evaporation of alcohol, the grid was examined by a Hitachi HS-7D electron microscope.

5.3 Raman Spectra of Germanium Particles in Thin Film

The typical Raman spectra of evaporated Ge films annealed thermally are shown in Fig. 5.1. In the middle part of this figure, two spectra resolved into the crystalline mode ($\sim$ 300 cm^{-1}) and the amorphous-like one ($\sim$ 280 cm^{-1}) are also plotted. The volume fraction of crystallinity v_f can be determined from the integrated intensities of the crystalline and amorphous-like modes by using the same method discussed in § 3.3.

Then we apply v_f to the Avrami formula eq. (3.3) to analyze the structural changes. The Arrhenius plots of $\ln[(1 - v_{f0})/(1 - v_f)]$ are shown in Fig. 5.2. It is evident that the structural change of evaporated Ge films is well described by the same mechanism observed in the Si films (§ 3.3). Furthermore, from a least squares fit to the experimental points, the activation energy E_a is found to be 0.13 eV for the incipient stage regardless of the annealing time, and to be the value above 1.0 eV for the later stage dependently on the annealing time. It is noted that the energy of the incipient change agrees with the activation energy for the viscous flow of Ge, 0.14 eV (2.74 kcal/mol),[4] and that this result of the Ge film is consistent with that of evaporated Si film (see § 3.3).

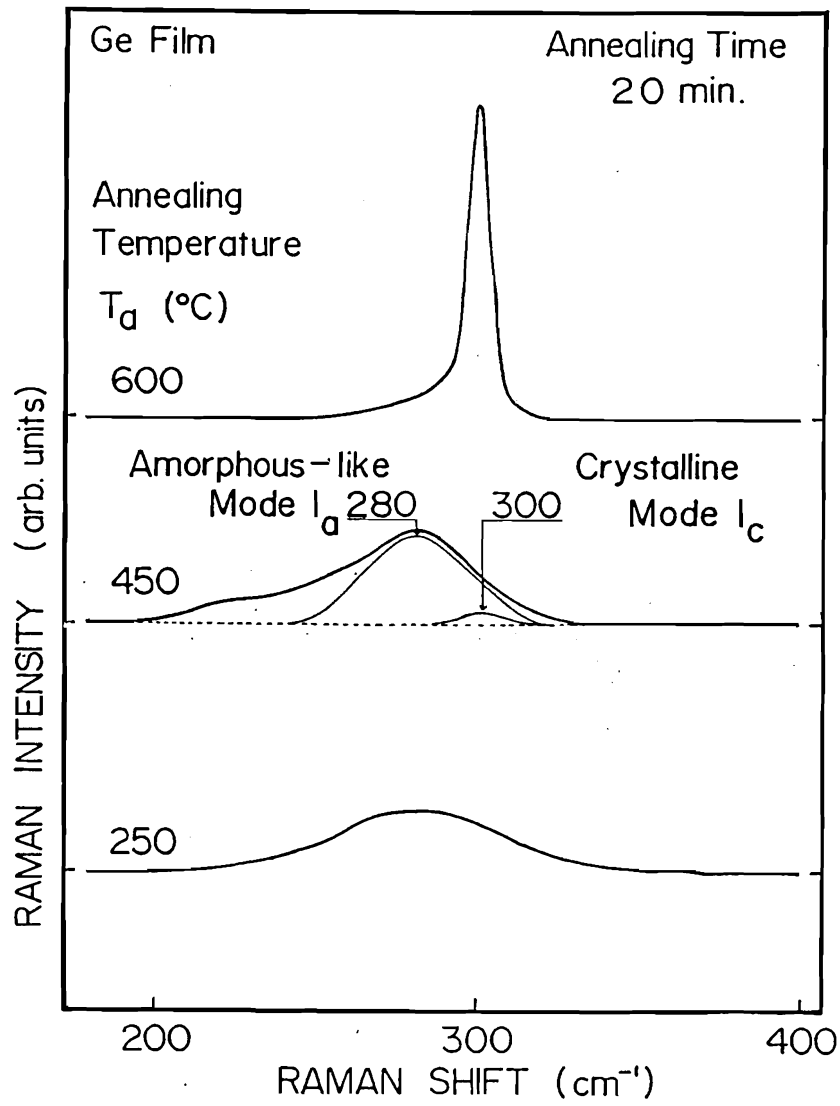

Fig. 5.1 Typical Raman spectra of evaporated germanium films annealed at temperature 250, 450 and 600 °C. The middle part contains two resolved spectra of the crystalline mode and the amorphous-like one.

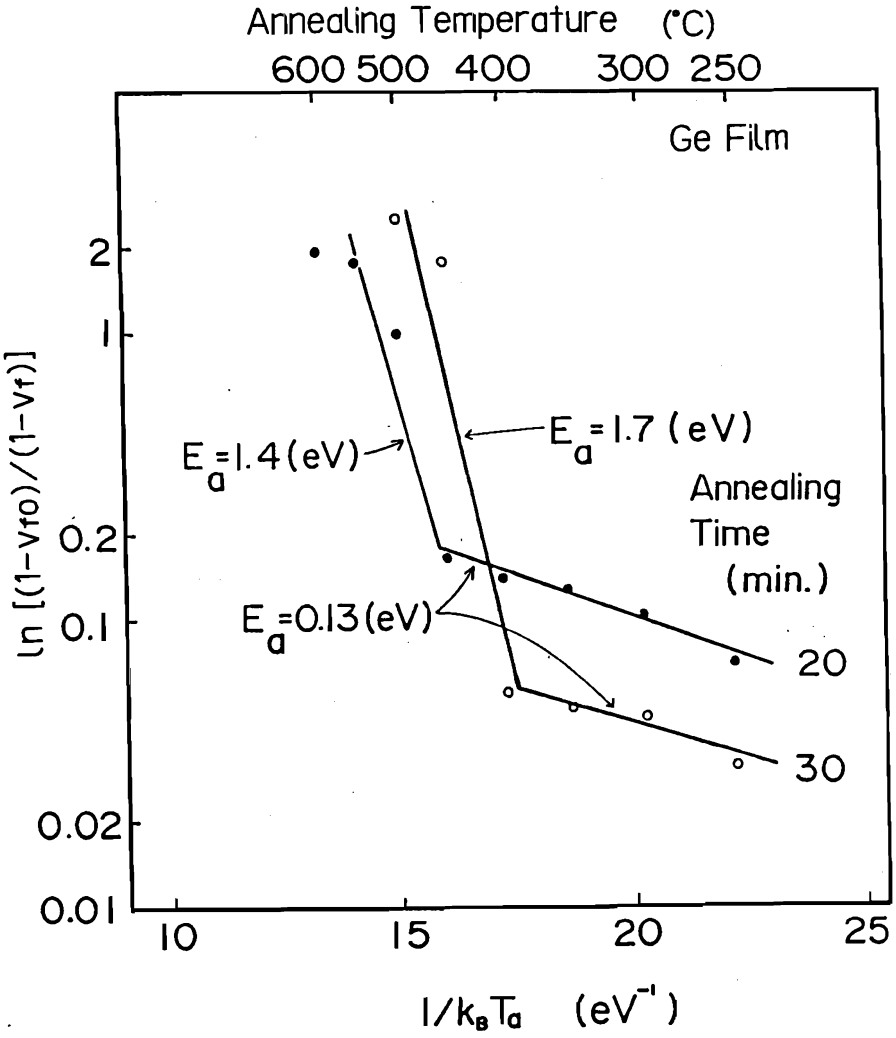

Fig. 5.2 Arrhenius plots of $\ln[(1 - v_{f0})/(1 - v_f)]$ versus inverse temperature for samples annealed for 20 and 30 minutes. The solid lines are least-squares fits to the experimental points.

To our knowledge the value of 0.13 eV for the incipient stage is the lowest energy in the crystallization energies of Ge films reported previously, which have scattered in a wide range from 0.18 to 3.2 eV.[5-10] One reason why we observe the lowest value is that the Raman scattering is very sensitive to variations in structural order of so-called amorphous state. In fact the study using the Raman linewidth on annealed amorphous Ge and Si films has determined a value for the structural relaxation energies of about 0.2 eV for both Ge and Si,[9,10] which are the closest values to the present result in the literature. And the other energies determined by using the other techniques are higher than those values.

5.4 Raman Spectra of Germanium Particles with Free Boundary

Figure 5.3 shows the dependence of the Raman spectrum of the gas-evaporated Ge particles on the annealing temperature T_a. We can see that the as-deposited sample shows a broad Raman band at around 280 cm^{-1}, the amorphous-like component. It should be noted that the appearance of the amorphous-like component does not always imply the random network structure of materials studied; gas-evaporated Si and Ge particles smaller than about 100 Å usually show this amorphous-like component, even though high resolution electron microscopic observations prove that they are crystalline.[11,12] Our measurement of the average particle size from the electron micrographs shows that the as-deposited sample contain crystalline particles as small as 90 Å.

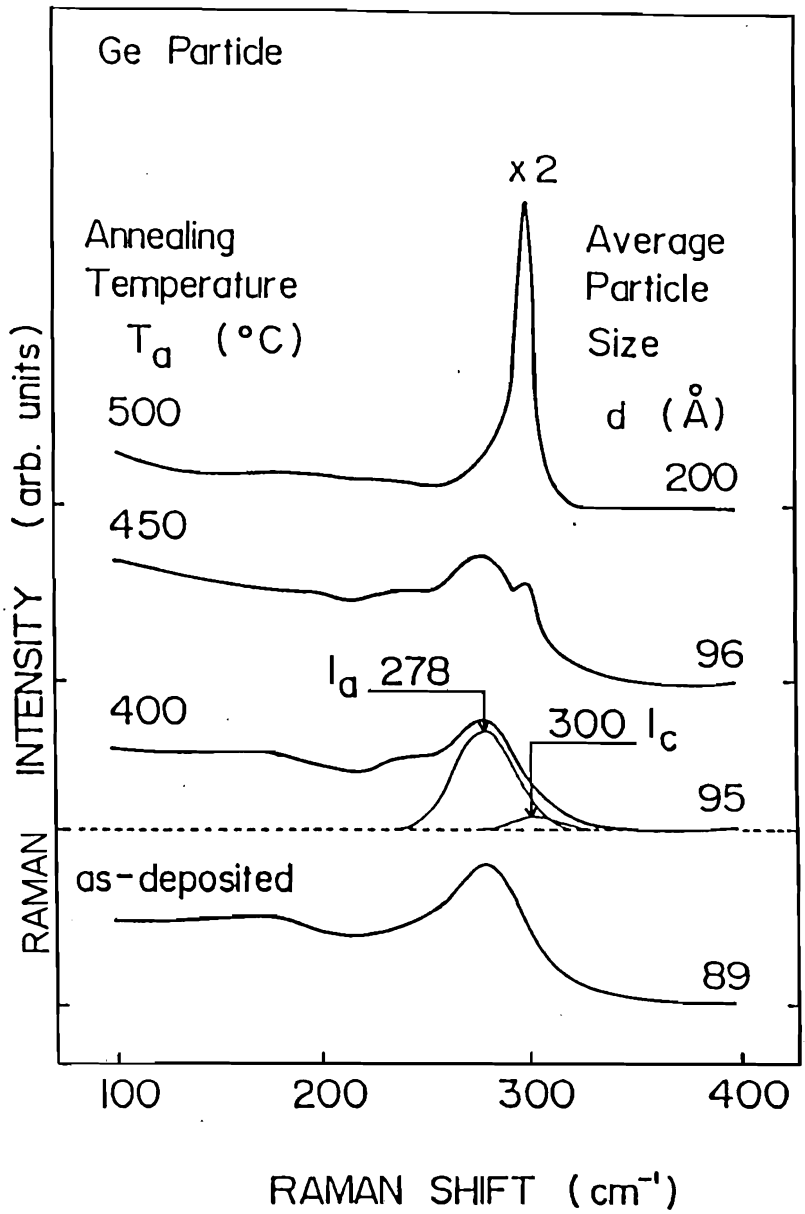

Fig. 5.3 Dependence of Raman spectra from the small germanium particles on the annealing temperature T_a. An example of the decomposition of the spectrum into the crystalline and amorphous-like modes is shown for the spectrum T_a = 400 °C.

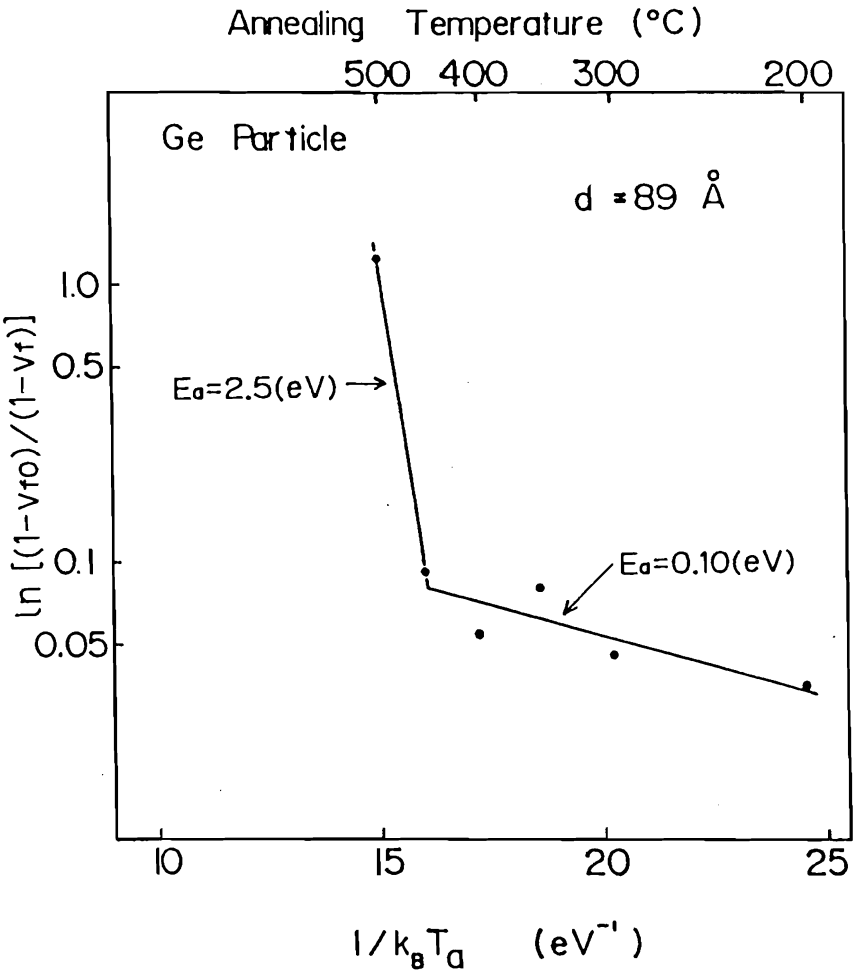

Fig. 5.4 Arrhenius plot of $\ln[(1 - v_{f0})/(1 - v_f)]$ obtained by analyzing the Raman spectra of the small germanium particles shown in Fig. 5.3.

When $T_a \leqq 450$ °C, no drastic change in the Raman spectrum is observed, even though a small peak at round 300 cm^{-1} appears at $T_a = 450$ °C. The most drastic change in the spectrum occurs when T_a is raised to 500 °C; the crystalline peak at around 300 cm^{-1} grows abruptly and the amorphous-like component becomes very weak. We note here that the spectral changes presented in Fig. 5.3 for the Ge particles resemble very much those previously reported for thermally annealed Si (§ 3.3) and Ge (§ 5.3) films.

Following the same manner as applied to the analysis of the structural change of Si film (§ 3.3), we deduced the volume fraction of crystallinity v_f, then plotted $\ln[(1 - v_{f0})/(1 - v_f)]$ as a function of $1/k_B T_a$ (Arrhenius plot). This is shown in Fig. 5.4 indicating the close similarity between the spectral changes seen for the Ge particles with free boundary and the Si and Ge particles in thin films. We can see that the plot is folded at the temperature where the strong crystalline Raman peak abruptly emerges. For the present Ge particles, we obtain the low activation energy $E_a = 0.10$ eV, which is slightly lower than that for the Ge film (0.13 eV). We also obtain the high activation energy $E_a = 2.5$ eV, which is slightly higher than that for the Ge film (1.4 eV). It should be stressed that although the values of the activation energy obtained are slightly different from those for the Ge film, the Arrhenius plot obtained is very similar to that for the Ge film.

The spectral changes observed in Fig. 5.3 are correlated with the electron micrographs of the Ge particles before and after the thermal annealing. Form the electron micrographs measured, we observed that when $T_a \leqq 450$ °C the particle size remains almost same, while at $T_a = 500$ °C the particle size in-

creases abruptly. We determined the average particle size d directly from the electron micrographs by measuring the linear dimension of particles along only one direction of the micrographs. The average determined by this procedure implies the rotational average as well as the average over the size distribution as mentioned in § 2.3. The average particle sizes obtained are d = 89 Å for the as-deposited sample and d = 95, 96 and 200 Å for the samples annealed at T_a = 400, 450 and 500 °C, respectively. Note that the particles become about two times larger than before when annealed at 500 °C.

The above experimental results indicate that an abrupt growth of the Ge particles occurs between T_a = 450 and 500 °C, at a temperature much lower than the melting point of bulk Ge (934 °C); the abrupt growth of the particles leads to an abrupt increase in the intensity of the crystalline Raman signal and also results in the folding of the Arrhenius plot.

5.5 Interpretation of Structural Change of Ge and Si Particles

Our finding of the two-step structural change is common to the Ge particles with free boundary (§ 5.4), the Ge film (§ 5.3) and the Si film (§ 3.3). So we discuss here possible mechanisms of this phenomenon simultaneously.

In order to interpret this structural change, we accept the microcrystalline model instead of the continuous random network model as the structure of amorphous semiconductors. Recent observations by high resolution electron microscopy (HREM) have given the direct evidence of the validity of the microcrystalline model: (1) Saito[12] showed about 14-A submicrocrystallites in plan-view lattice images of vacuum-deposited Ge films. (2) Ourmazd *et al.*[13] reported 15- 30-A submicrocrystallites in *a*-Si

observed HREM lattice imaging in cross section of Si films. (3) Phillips *et al.*[14] supported the microcrystalline model on the basis of the observation of Bragg diffraction from super-nanometer regions of so-called amorphous Si, which reveals the existence of crystalline clusters too small to be observed by X-ray diffraction in bulk. The lattice fringes have also been observed by HREM for gas-evaporated particles of Si and Ge,[10] and amorphous films other than Si and Ge such as SiO,[16] WO_3[17] and SiGe.[18] It is noted that these results obtained through HREM are consistent with our conclusion presented in this thesis up to now.

At first, we discuss the incipient stage with the low activation energy based on the microcrystalline model. Our results indicate that the crystallite size remains almost the same in the temperature range interested here. Therefore, we believe that the process involves the rearrangement of surface atoms. We postulate that the film is composed of microcrystals having slightly-deviated or distorted atoms at surface layers. Thus the microcrystals can be restricted easily by ordering of the surface atoms from low temperature at a constant rate of low energy. We presume this ordering to, especially, be a decrease in bond angle deviation.

The above assumption is supported by indirect evidence extensively. (1) Extended X-ray-absorption fine-structure (EXAFS) measurements on amorphous Ge showed the increase of the second-neighbor peak strength with an augment of the local order,[8,19-21] The second peak was considered to be a measure of the tetrahedral angle distribution. Therefore, since the incipient change arises from ordering of the bonding angle, it is reasonable that the energy requisite to the variation in bonding

angle is much lower than a covalent bond energy that corresponds to changes in the first-neighbor distance. (2) It was reported that changes in the bond angle width of 7 %, which is a practical value of the bond angle deviation, result in the difference in optical gap of 0.2 eV between amorphous Ge films deposited at different substrate temperature.[22] (3) The Raman linewidth of the optic peak was applied to the determination of an activation energy for structural relaxation of amorphous films.[9,10] This determination is based on the argument that the width of the optic peak increases roughly linearly with the root-mean-square bond angle deviation.[23] The determined values (about 0.2 eV) of the activation energy are close to our values. All the above results confirm our assumption in conjunction with one another. However these are only indirect evidence, thus further investigation treating our opinion as well as the other possibility such as a wurtzite to diamond transformation[15] is very desired to settle the structural model.

We now turn our attention to the latter stage, especially to the abrupt particle growth observed between T_a = 450 and 500 °C for the Ge particles. We believe that the presently observed particle growth can be well explained by the low temperature coalescence of of particles, which is extensively studied in connection with the growth mechanism of smoke particles.[24-26] In the gas-evaporation process, the coalescence growth takes place in a convection stream of inert gas, in such a way that the smoke particles collide with each other and then unite with one another in a definite orientation to minimize their interface energy. Kaito[26] studied in detail the growth mechanisms of Ag particles by allowing the smoke to pass a heater. He showed that the liquid-like coalescence (fusion) occurs at 400 °C and

the surface-melting coalescence at 270 °C. It should be noted that these coalescence temperatures are much lower than the melting point of bulk Ag (962 °C). In our annealing experiments, the growth of Si and Ge particles takes place on the substrate, not in the convection stream of gas. However the coalescence growth is possible, because the particles are so densely collected or packed that they touch one another.

As theoretically demonstrated,[27,28] the melting temperature and the Debye temperature of small particles are expected to be lower than the bulk ones because of the large anharmonicity in the lattice vibration. If we adopt the Lindeman's melting formula[29] for simplicity, the ratio of the melting temperature of a small particle T_p to that of a bulk crystal T_b can be expressed as $T_p/T_b = (\theta_p/\theta_b)^2$, where θ_p and θ_b are the Debye temperatures of the particle and of the bulk crystal, respectively. Inserting a value of θ_p determined for Ag smoke from X-ray measurement,[30] Kaito could obtain a value of T_p, which agrees very well with his experimental liquid-like coalescence temperature. Furthermore, using values of the surface Debye temperature determined from low-energy electron diffraction (LEED) measurements,[31] he could show that the surface melting coalescence occurs by the connection of (100) planes.

For the present Ge particles, we cannot precisely determine which of two coalescence modes, the liquid-like coalescence or the surface melting coalescence, takes place. However, a fact that the particles observed by electron micrographs appear to be more or less elongated suggests that the surface melting coalescence rather than the liquid-like coalescence takes place, because the liquid-like coalescence may result in spherical particles as pointed by Kaito.[26] After our experimental results,

we can approximately set T_p = 748 K (475 °C), the temperature at which the coalescence takes place. Then, inserting T_b = 1209 K and θ_b = 378 K for bulk Ge[4] into the above relation, we can obtain a rough estimate of the Debye temperature of small Ge particles as θ_p = 295 K. To our knowledge, neither the X-ray data nor the LEED data, which allow us to estimate the Debye temperature of Ge particles, are available. It is of great interest to perform X-ray and LEED experiments on Ge and to compare the results with the above estimate of θ_p.

We finally discuss the crystallization process of so-called amorphous Si and Ge films. As mentioned in before, the dependence of Raman spectrum on the annealing temperature and the Arrhenius plot obtained for the Ge particles with free boundary is very similar to that obtained for *a*-Si and *a*-Ge films. This close similarity allows us to assume that nearly the same phenomena occur in both the gas-evaporated microcrystals and so-called amorphous films. As pointed out at the beginning of this section, the recent HREM observation indicates that the so-called amorphous films are composed of extremely small microcrystals. At least qualitatively, these microcrystals in the films are expected to behave like the particles with free boundary. From the present results, we can attribute the crystallization process with high activation energy to the coalescence growth of the microcrystals.

The activation energy obtained for the Ge particles (E_a = 2.5 eV) is slightly higher than that obtained for *a*-Ge films (E_a = 1.4 eV). This quantitative difference may arise from the difference in the crystallite size before annealing and the boundary condition at the particle surface. In fact, our as-deposited sample contains the crystallite of the order of 90 Å in size,

while those in *a*-Ge films are reported to be of the order of 14 Å.[13] In addition, the Ge particles have free surfaces and contaminations around the particles such as oxygen atoms may prevent the coalescence, while microcrystals in *a*-Ge films are closely packed and the bonding between adjacent microcrystals may exist to some extent. Smaller microcrystals may coalesce more easily. Furthermore, the partial bonding between adjacent microcrystals may facilitate the coalescence. Thus the microcrystals in so-called amorphous Ge films can grow with an activation energy lower than that for the Ge particles with free boundary.

5.5 Summary

In this chapter, we dealt mainly with Ge particles both with free boundary conditions and in thin film. The analytical method was the same as used for the Si particles.

The structural changes were observed for the Ge particles both with free standing and those closely packed in thin film. That is, two-step changes were detected in the Arrhenius plots obtained by resolving the Raman spectra of the samples annealed thermally, indicating the similarities between Si and Ge.

On the basis of the microcrystalline model, these structural changes were explained for the Si and Ge particles with free boundary conditions and in thin films simultaneously. We suggested that the incipient stage with the low activation energy arises from the ordering of the surface atoms, and that the abrupt particle growth of the latter stage with high activation energy is attributed to the coalescence of the particles.

References

1) S. Hayashi, M. Ito and H. Kanamori: Solid State Commun. 44 (1982) 75.

2) T. Okada, H. Wakayama, H. Kasahara and K. Yamamoto: J. Phys. Soc. Jpn. 55 (1986) 1415.

3) S. Hayashi, H. Wakayama, T. Okada, S. S. Kim and K. Yamamoto: J. Phys. Soc. Jpn. 56 (1987) 243.

4) A. J. Moses: *The Practicing Scientist's Handbook* (Van Nostrand Reinhold, New York, 1978) p.1021.

5) A. Barna, P. B. Barna and J. F. Pocza: J. Non-Cryst. Solids 8-10 (1972) 36.

6) K. L. Chopra, H. S. Randhawa and L. M. Malhotra: Thin Solid Films 47 (1877) 203.

7) P. Germain, S. Squelard, J. Bourgoin and A. Gheorghiu: J. Appl. Phys. 48 (1977) 1909.

8) M. A. Paesler, D. E. Sayers, R. Tsu and J. G.-Hernandez: Phys. Rev. B 28 (1983) 4550.

9) R. Tsu, J. G.-Hernandez and F. H. Pollak: J. Non-Cryst. Solids 66 (1984) 109.

10) R. Tsu, J. G.-Hernandez and F. H. Pollak: Solid State Commun. 54 (1985) 447.

11) S. Hayashi and H. Abe: Jpn. J. Appl. Phys. 23 (1984) L824.

12) S. Hayashi: Solid State Commun. 56 (1985) 375.

13) Y. Saito: J. Phys. Soc. Jpn. 53 (1984) 4230.

14) A. Ourmazd, J. C. Bean and J. C. Phillips: Phys. Rev. Lett. 55 (1985) 1599.

15) J. C. Phillips, J. C. Bean, B. A. Wilson and A. Ourmazd: Nature 325 (1987) 121.

16) C. Kaito and T. Shimizu: Jpn. J. Appl. Phys. 23 (1984) L7.

17) C. Kaito, T. Shimizu, Y. Nakata and Y. Saito: Jpn. J. Appl.

Phys. 24 (1985) 117.

18) S. Hayashi, M. Fujii, T. Takanabe and K. Yamamoto: Jpn. J. Appl. Phys. 27 (1988) L1165.

19) F. Evangelisti, M. Gsrozzo and G. Conte: J. Appl. Phys. 53 (1982) 7390.

20) F. Evangelisti, M. G. Proietti, A. Balzarotti, F. Comin, L. Incoccia and S. Mobilio: Solid State Commun. 37 (1981) 413.

21) E. A. Stern, C. E. Bouldin, B. von Roedern and J. Azoulay: Phys. Rev. B 27 (1983) 6557.

22) J. S. Lannin, N. Maley and S. T. Kshirsagar: Solid State Commun. 53 (1985) 939.

23) D. Beeman, R. Tsu and M. F. Thorpe: Phys. Rev. B 32 (1985) 874.

24) S. Yatsuya, S. Kasukabe and R. Uyeda: Jpn. J. Appl. Phys. 12 (1973) 1675.

25) C. Kaito: Jpn. J. Appl. Phys. 17 (1978) 601.

26) C. Kaito: Jpn. J. Appl. Phys. 24 (1985) 261.

27) A. Nakanishi and T. Matsubara: J. Phys. Soc. Jpn. 39 (1975) 1415.

28) T. Matsubara: J. Phys. Soc. Jpn. 40 (1976) 603.

29) J. M. Ziman: *Principles of the Theory of Solids* (Cambridge Univ. Press, Cambridge, 1965) p.323.

30) Y. Kashiwase, I. Nishida, Y. Kainuma and K. Kimoto: J. Phys. 38 (1977) 157.

31) J. M. Morbito, Jr., R. F. Steiger and G. A. Somorjai: Phys. Rev. 179 (1969) 638.

Chapter 6

Conclusions

A systematic study has been carried out on the small semiconductor particles of Si and Ge by using Raman scattering spectroscopy in combination with electron microscopy. There have been main two purposes of this thesis work: One is to investigate finite-size effects on the vibrational modes in nonpolar semiconductors. The other is, by extending the consideration on the small particles to an amorphous semiconductor field, to contribute to the study of the structure of amorphous Si and Ge. For our purpose, Raman scattering has been a powerful tool because of its sensitivity and adaptability to the semiconductors of Si and Ge. The Raman spectra from the gas-evaporated Si particles with free boundary conditions have been measured and analyzed by comparing with the Si microcrystals packed in thin film. The structural changes induced by, mainly, thermal annealing have been detected by the Raman scattering measurements. We have also made a comparison between Si particles with Ge ones. The main results obtained in this thesis work are summarized as follows:

(1) The average particle size d of gas-evaporated Si particles determined from the micrograph varied from 70 to 220 Å, and the particle-size distribution was analyzed. We found that the size distribution is well described by a log-normal distribution function. The geometric standard deviation in the log-normal distribution function of the Si particles agrees with an empirical rule for the width of the distribution; this deviation has to fall within a band given by $\sigma = 1.48 \pm 0.2$ for crystalline inert-gas-evaporated particles. The electron diffraction patterns showed clear Debye-Scherrer

rings indicting that the Si particle possess the same crystalline structure as the bulk Si.

(2) The Raman spectra of the Si particles changed from an amorphous-like broad spectrum (d = 70 Å) to a mixed spectrum with crystalline and amorphous-like phases (d = 220 Å). It was noted that the silicon particles as small as 100 Å show an amorphous-like Raman spectrum even though their structure is crystalline. The Raman spectra were resolved into four modes in the rage of 250 to 600 cm^{-1}; these were identified to the LA- ($\sim$ 300 cm^{-1}) and TO- ($\sim$ 480 cm^{-1}) like modes observed in so-called amorphous Si, the allowed-TO-phonon mode ($\sim$ 520 cm^{-1}) of crystalline Si, and a new surface mode ($\sim$ 430 cm^{-1}).

(3) In order to check the structure of the silicon particle, the thermal annealing and laser irradiation experiments were made. For the isochronal annealing of the Si particles, the small change was observed and attributed to the formation of Si-O bond on the surface. On the other hand, the sharp crystalline peak on the Raman spectrum induced by the the laser irradiation was well analyzed by using the theoretical calculation for bulk Si. It was concluded that the change observed in the Raman spectrum of the small silicon particles during laser irradiation is caused by a temperature rise in the same manner as that which takes place in bulk Si.

(4) Structural changes of evaporated Si films induced by thermal annealing were measured by Raman scattering. The volume fraction of crystallinity v_f of the film was determined from the integrated intensities of a crystalline and an amorphous-like components. v_f was then applied to the Avrami formula, which express a process activated thermally with a

single activation energy at a fixed temperature. We found that the two-step structural change with activation energies of 0.35 and 0.87 eV, and that the low energy of 0.35 eV is identical to the activation energy for the viscous flow of Si, 0.37 eV (8.63 kcal/mol).

(5) The Raman scattering study was extended to glow-discharge(GD)-deposited Si films. The dependence of preparation parameters of RF power and DC bias voltage on the structural properties was discussed by using v_f, the linewidth of the Raman spectrum, and the crystallite size determined from X-ray diffraction. In order to interpret the finite-size effect of small particles formed in the film, we compared our experimental results of evaporated and GD-deposited Si films with the theoretical calculation made by Richter *et al.*, and pointed out that the finite-size effects of the small particles with free boundary are not explained by the relaxation of the wave-vector selection rule only.

(6) The Raman depolarization ratio ρ of small Si particles with an average particle size from 60 to 350 Å was reported for the first time. The low values of ρ for the particles having a crystalline peak were not explained by regarding the particles as the bulk Si. Thus bulk concepts such as the F_{2g} symmetry and k-selection rule are inoperative to the small silicon particles. By comparing ρs of the silicon particles with those of films, we showed that the broad amorphous-like spectra do not mean the continuous random network structure or molecular-like cluster. The experimental results presented here were not predicted by existing theories.

(7) Germanium particles both with free boundary conditions and

in thin film were studied by using the same analytical method as used for the Si particles. We found that the two-step changes observed in the Arrhenius plot obtained by resolving the Raman spectra of the samples annealed thermally, indicating the similarities between Si and Ge. The activation energies obtained were 0.10 and 2.5 eV for the Ge particles, and 0.13 and 1.4 eV for the evaporated Ge film. It was noted that the energy of the incipient change agrees with the activation energy for the viscous flow of Ge, 0.14 eV (2.74 kcal/mol), and that this result of the Ge film is consistent with that of the evaporated Si film.

(8) Possible mechanisms of the two-step structural change, which is common to the Ge particles with free boundary, the Ge film and the Si film, were discussed based on the microcrystalline model instead of the continuous random network model as the structure of amorphous semiconductors. We suggested that the incipient stage with the low activation energy results from the rearrangement of surface atoms, and the crystallization process with high activation energy was attributable to the coalescence growth of the microcrystals.

Vita

Tadashi Okada was born in Tsuyama, Okayama, Japan, on March 1, 1951. He graduated from Tsuyama National College of Technology, Tsuyama, in March of 1971. He jointed New Nippon Electric Company, Ltd., in April of that year, and spent four years developing and manufacturing power transistors and ICs. He became a faculty member of Tsuyama National College of Technology in April of 1975, and studied as a research worker at Kobe University from May of 1983 till February of the next year. He is currently a Lecturer in the Department of Electronics and Computer Engineering, Tsuyama National College of Technology.

He is a member of the Physical Society of Japan, the Japan Society of Applied Physics, the Institute of Electronics, Information and Communication Engineers of Japan, and the Information Processing Society of Japan.